International Journal of Plasticity 25 (2009) 1655–1683

Contents lists available at ScienceDirect

International Journal of Plasticity

journal homepage: www.elsevier.com/locate/ijplas

The role of heterogeneous deformation on damage nucleation at grain boundaries in single phase metals

T.R. Bieler [a,b,*], P. Eisenlohr [a], F. Roters [a], D. Kumar [b], D.E. Mason [c], M.A. Crimp [b], D. Raabe [a]

[a] Max-Planck-Institut für Eisenforschung, Max-Planck Strasse 1, 40237 Düsseldorf, Germany
[b] Chemical Engineering and Materials Science, 2527 Engineering Building, Michigan State University, East Lansing, MI 48824-1226, USA
[c] Mathematics and Computer Science, Albion College, Albion, MI 49224, USA

ARTICLE INFO

Article history:
Received 31 January 2007
Received in final revised form 28 August 2008
Available online 25 September 2008

Keywords:
Grain boundaries
Microcracking
Twinning
Finite elements
Crystal plasticity

ABSTRACT

The mechanical response of engineering materials evaluated through continuum fracture mechanics typically assumes that a crack or void initially exists, but it does not provide information about the nucleation of such flaws in an otherwise flawless microstructure. How such flaws originate, particularly at grain (or phase) boundaries is less clear. Experimentally, "good" vs. "bad" grain boundaries are often invoked as the reasons for critical damage nucleation, but without any quantification. The state of knowledge about deformation at or near grain boundaries, including slip transfer and heterogeneous deformation, is reviewed to show that little work has been done to examine how slip interactions can lead to damage nucleation. A fracture initiation parameter developed recently for a low ductility model material with limited slip systems provides a new definition of grain boundary character based upon operating slip and twin systems (rather than an interfacial energy based definition). This provides a way to predict damage nucleation density on a physical and local (rather than a statistical) basis. The parameter assesses the way that highly activated twin systems are aligned with principal stresses and slip system Burgers vectors. A crystal plasticity-finite element method (CP-FEM) based model of an extensively characterized microstructural region has been used to determine if the stress–strain history provides any additional insights about the relationship between shear and damage nucleation. This analysis shows that a combination of a CP-FEM model augmented with the fracture initiation parameter shows

* Corresponding author. Address: Chemical Engineering and Materials Science, 2527 Engineering Building, Michigan State University, East Lansing, MI 48824-1226, USA. Tel.: +1 517 353 9767; fax: +1 517 432 1105.
E-mail address: bieler@egr.msu.edu (T.R. Bieler).

0749-6419/$ - see front matter
doi:10.1016/j.ijplas.2008.09.002

promise for becoming a predictive tool for identifying damage-prone boundaries.

1. Introduction

Continuum fracture mechanics has provided a wealth of methodologies for modeling the evolution of damage, but these methods all depend on knowing where the damage nucleated; hence a pre-existing void or crack is normally introduced arbitrarily. The process by which undamaged material develops damage (here defined as the generation of a new free surface where there was none before) is not very well understood. An understanding of this damage nucleation process in the context of microstructural evolution will allow properties that are of great importance to designers, such as toughness, ductility, and fatigue life, to become more predictable. Damage nucleation frequently develops in two stages, where nascent or pre-damage conditions develop during monotonic deformation resulting from forming operations, followed by growth to a critical size during service, e.g. growth of short cracks at a scale smaller than the grain size, to one larger than the microstructural scale during subsequent loading. In this case nucleation and growth of fatigue cracks depends strongly on microstructure evolution during prior forming history. Thus, a paradigm is needed to understand how the process of plastic deformation interacting with microstructural features leads to the development of subcritical cracks or voids.

From both experimental and computational studies, it is commonly held that damage nucleation occurs in locations of large strain concentrations (from the continuum perspective, as in Fig. 1a), or microstructurally, where substantial heterogeneous deformation occurs. If large local strains are effective in accommodating required geometry changes they may prevent damage nucleation, whereas it is conceivable that damage may nucleate where insufficient strain or shape accommodation occurs, as illustrated schematically in Fig. 1b. Such variability in shape accommodation is connected to crystal orientations and crystallographic deformation mechanisms. Experimentally, heterogeneous deformation is often assessed using slip trace analysis, which can be accomplished with both optical and electron microcopy, and can be greatly enhanced and made more quantitative by using tools such as orientation imaging microscopy and strain mapping. However studies that fully analyze the operating deformation mechanisms in the context of the stress–strain history and observed microstructure evo-

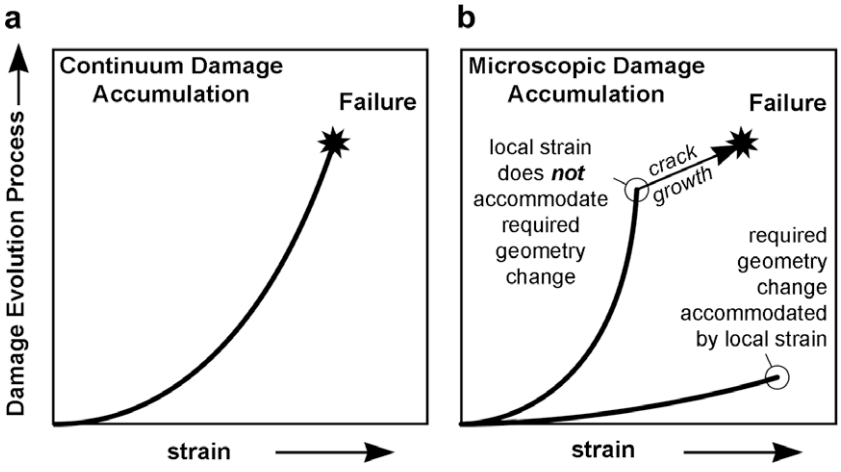

Fig. 1. Schematic depiction of relationship between damage and strain in a continuum sense (a), and a comparison of two microstructural scenarios where localized strain causes or prevents damage (b).

lution are rare. More qualitative experiments commonly show cracks and voids developing preferentially in some boundaries but less in others, indicating the significance of heterogeneity in local deformation history.

Computationally, two approaches to modeling evolution of microstructure have developed, statistical methods based upon Taylor theory, and finite element polycrystal plasticity approaches (atomistic or discrete dislocation density models can typically model volumes much smaller than a cubic micron (e.g. Farkas, 2005; Arsenlis et al., 2004), making them most useful for modeling nanocrystals). Statistical models developed on the foundation of Taylor theory (e.g. Chen and Gray, 1996; Nemat-Nasser et al., 1998; Nemat-Nasser and Guo, 2000) homogenize deformation characteristics, which is useful for modeling deformation phenomena at the scale of forming operations. This kind of analysis motivates models for yield surface evolution, e.g. Barlat et al. (2003). Homogenization is not helpful for investigating damage nucleation, however, which is a statistically rare event that reflects deviations from homogeneous behavior. This shortcoming can be partially overcome using viscoplastic self-consistent polycrystal plasticity codes that allow strains and stresses to vary in different crystal orientations (e.g. Lebensohn and Tome, 1993; Lebensohn, 2001; Karaman et al., 2000). Nevertheless, self-consistent codes are still based upon a statistical representation of a microstructure. Hence, damage that originates from strain incompatibilities in specific sites cannot be meaningfully predicted with statistical models such as the large body of literature based upon continuum damage mechanics (e.g. review of Lin et al., 2005), because the specific strain history depends on both the local strain behavior near an interface, as well as the strain history in adjacent grains or even within regions of the same grain (non-local strain). Self consistent models homogenize the grain neighborhood and, therefore, cannot provide detailed information at the local scale.

Modeling of site-specific stress–strain histories can be accomplished with crystal plasticity finite element modeling of representative microstructural volumes (oligocrystals or microstructure patches). Several approaches have recently been developed and compared with experimental observations (e.g. Hao et al., 2003, 2004; Heripre et al., 2007; Querin et al., 2007; Dunne et al., 2007; Clayton and McDowell, 2004; Bhattacharyya et al., 2001; Raabe et al., 2001; Ma and Roters, 2004; Ma et al., 2006a,b, Zaafarani et al., 2006, Cheong and Busso, 2004, 2006, Dawson et al., 2002, Kalidindi and Anand, 1993). To date, most modeling attempts of this kind have simulated high ductility damage resistant metals such as steel, copper, or aluminum. Characterizing damage nucleation events microscopically in such high ductility metals is challenging due to the large strains and high dislocation densities that precede damage nucleation.

The ability to predict damage nucleation and evaluate whether it will lead to the fatal flaw is one of the major goals of computational plasticity. Such predictions require multiscale modeling approaches that are under development in a number of groups and laboratories (Hao et al., 2003, 2004; Clayton and McDowell, 2004; Voyiadjis et al., 2004; Buchheit et al., 2005; Dunne et al., 2007; Cheong et al., 2007). While heterogeneous deformation is understood to be a precursor to damage nucleation, *the actual initiation step* between heterogeneous deformation and damage nucleation is not clearly understood. This connection is crucially important, because if the locations of damage are not properly predicted, then any simulations of microstructural evolution that evolve thereafter will be unreliable (merely fiction). A comprehensive review of multi-scale modeling of plastic deformation shows that solutions to practical problems often have the nanoscale effectively interacting with microscale, which cannot be handled by atomistic methods (Liu et al., 2005, Hao et al., 2003, 2004). Currently, there are no effective handoff methods between atomistic and microstructure scales. Hence, there is an opportunity for bridging across length scales if damage nucleation (intrinsically a nano-scale phenomenon) can be predicted reliably on the basis of heterogeneous microscale deformation.

Interfaces represent a profound challenge to modeling heterogeneous deformation and damage nucleation. Damage in particle-free materials normally nucleates at discontinuous interfaces such as grain or phase boundaries.[1] At interfaces, strain must be somehow transferred from one grain to another through the boundary. In this process, damage may nucleate at a specific (rather than a generic)

[1] Hard particles are often the source of pre-existing damage, which can crack with deformation processing.Damage evolution based on such sources has been modeled by many investigators, as it can be philosophically consistent with the statistical approaches of continuum damage mechanics, which is beyond the scope of this paper.

interface, due to both local and non-local effects. Rules for predicting which interfaces become damage nucleation sites are not known, though some have used slip transfer criteria as a means to identify suspicious locations (e.g. Ashmawi and Zikry, 2003a,b). From the review that will follow, it will become clear that damage nucleation at interfaces depends on

i. the orientations of crystals on either side of the interface,
ii. the boundary orientation and structure (energy),
iii. the activated deformation systems on either side of the boundary, and
iv. the stress–strain gradient history in the grains on either side of an interface.

Research that considers all four of these factors is rare. For example, the *grain boundary engineering* paradigm focuses on grain boundary energy (item ii) as a metric for "good" or "bad" grain boundaries, but little has been done to examine how slip processes affect the character of "good" Σ boundaries differently from their "bad" random boundary counterparts. Item iii has rarely been examined experimentally or computationally, and when it has, it has not been done with fine detail. Studies of deformation transfer have led to identification of some rules by which a dislocation in one grain can penetrate into a neighboring grain (Clark et al., 1992; de Koning et al., 2002, 2003). However, it is not clear how deformation transfer and damage nucleation are related, and this open question provides the primary motivation for this paper. Clearly, knowledge of a boundary's propensity to generate damage could provide an effective bridge between atomistic and continuum scale models.

To assess the role of slip processes at interfaces on damage nucleation, it is important to have a reliable representation of heterogeneous deformation, the character of the grain boundary, and slip transfer mechanisms. These three topics and current approaches to integrate them are reviewed in some detail in order to provide motivation and a foundation for a new approach that identifies a deformation system based definition of grain boundary character. This new definition of grain boundary character was developed on the basis of experimental observations, and it may be able to determine which kind of deformation system interactions at the boundary will lead to damage nucleation. One example of a deeply characterized microstructure from this experimental work is examined using a current polycrystal plasticity finite element model to identify how mesoscale computational modeling may be used in combination with this new definition of grain boundary character to predict locations of damage nucleation.

1.1. Heterogeneous deformation in different grains

Analysis of heterogeneous strain near boundaries can be traced back to Livingston and Chalmers (1957), who observed that more slip systems are active near bicrystal grain boundaries than in the grain interior. However, bicrystals with arbitrarily oriented grains generally activate only one slip system in the grain interior (unless orientations are *chosen* that have the same Schmid factor for multiple slip systems), unlike polycrystals that generally require activation of two or more slip systems due to compatibility constraints. Thus, bicrystals will not typically generate deformation states that correspond to those found in polycrystal interfacial boundaries, and consequently cannot provide a reliable basis for predicting deformation conditions in polycrystals (though they can and have provided much insight and understanding about processes of deformation transfer).

Poly or multicrystal aluminum alloys and pure copper have been used for focused studies to characterize and model heterogeneous slip near grain boundaries (e.g. Yao and Wagoner, 1993; Delaire et al., 2000). Within a given grain, slip traces of deformation systems with high Schmid factors extended across grains, while planes with moderate Schmid factors had slip traces that extended part way from a boundary into the grain interior. Experimentally measured surface strain maps on high purity copper polycrystals show that heterogeneous strains extend 20–100 microns into the grain interior (Thorning et al., 2005; Clayton and McDowell, 2004). Local rotations have been measured using orientation imaging microscopy, which has allowed direct comparisons with polycrystal plasticity-finite element method (CP-FEM) models (Bhattacharyya et al., 2001; Raabe et al., 2001; Sachtleber et al., 2002; Tatschl and Kolednik, 2003; Prasannavenkatesan et al., 2005; Cheong and Busso, 2004, 2006; Cheong et al., 2007). Raabe et al. (2001) used a local micromechanical Taylor factor to better

predict local crystal rotations and strains that were measured using high resolution strain mapping techniques. Simulations of HCP metals and alloys have also been done (e.g. Barton and Dawson, 2001; Diard et al., 2005), though there is a lesser degree of direct comparison with experiment than with investigations on cubic metals. The FEM models generally assume no specific grain boundary properties such that the discontinuity of plastic properties accounts for the observed heterogeneous strain.

While boundaries clearly cause heterogeneous strain in adjoining crystals, it is not clear how this strain affects the cohesive properties of the grain boundary, because a strongly cohesive boundary *may* force heterogeneous strain in an adjacent grain in order to maintain compatibility. On the other hand, large heterogeneous strains may cause large tensile tractions in the boundary that could nucleate damage (e.g. Bieler et al., 2005a,b; Querin et al., 2007). Thus, the evolution of local stress–strain history and boundary properties will affect damage nucleation.

1.2. Grain boundary character and mechanical properties

A growing body of research has followed the paradigm that strong and weak grain boundaries can be identified based upon the structure of the boundary, i.e. grain boundary character (Watanabe, 1984). However, the fundamental meaning of strong and weak boundaries is not well defined. For example, a strong boundary may simply have a high cohesive strength, but such a boundary may not always be a strong barrier to dislocation motion (e.g. twins can either transmit dislocation slip easily or be a strong barrier, depending on the actual the slip system interaction). Thus, the idea of grain boundary strength can be approached from several perspectives.

Many studies have correlated properties of boundaries with their interfacial structure using the coincident site lattice (CSL) model, where a low Σ value indicates a high degree of common lattice points in adjacent grains. Beneficial properties of low Σ boundaries have been identified: Low Σ boundaries have low solubility for alloy or impurity elements, which makes them less susceptible to corrosion or nucleation of second phase particles (Palumbo et al., 1991; Watanabe, 2000; Lejcek and Hofmann, 2002; Lejcek et al., 2003; McMahon, 2004). Low Σ boundaries maintain their low energy configurations with a few degrees of deviation, accommodated by grain boundary dislocations (Brandon, 1966; Frary and Schuh, 2003). Materials with large numbers of low Σ boundaries (Palumbo et al., 1998, Kim et al., 2003, Watanabe and Tsurekawa, 2004; Randle, 2004) that are well connected in networks (Schuh, 2003, McGarrity et al., 2005) exhibit higher flow stress and ductility than materials with few low Σ boundaries. Because low Σ boundaries are less able to absorb lattice dislocations than random boundaries (Kokawa et al., 1981), many researchers have attributed material strength, and/or resistance to damage nucleation, to the presence of low Σ boundaries (Watanabe, 1984; Watanabe and Tsurekawa, 1999, 2005; Tsurekawa et al., 1999).

Another class of boundaries referred to as *special* boundaries have interfaces with low energy surfaces and repeating polyhedral structural units (generally a subset of low Σ boundaries). Of the five parameters that describe a boundary, three for the misorientation, and two for the boundary normal, low Σ boundaries are sufficiently defined by the misorientation. Many studies show that lowest energy configurations result when the boundary normal is a low index crystal plane, or has a common crystal direction about which there is a tilt or twist (Rohrer et al., 2004, 2006; Tschopp and McDowell, 2007; Wolf, 1990). Hence, low angle boundaries (referred to as $\Sigma 1$) are *special*. In analysis of beneficial grain boundary character, the most beneficial boundaries are found to those with low surface energy, which also have structural repeating polyhedral units in the boundary plane (Randle, 2001; Rohrer et al., 2006). Recent studies by Tschopp et al. (2007, 2008) have shown that dislocation emission is correlated with the presence of particular kinds of polyhedral structural units.

However, low Σ or *special* boundary attributes are neither a necessary nor sufficient definition of a strong or beneficial boundary. First, the beneficial effect of these boundaries cannot be exclusively ascribed to lower solute content, because solute atoms can also strengthen grain boundaries, e.g. B doping in aluminides. Second, even though the benefit of such boundaries is statistically convincing, some low Σ boundaries do develop damage, while many more random boundaries do not (e.g. Lehockey and Palumbo, 1997), suggesting that additional criteria for identifying strong and weak boundaries exist, such as the influence of active deformation systems. There is little study of effects of deformation

systems on boundary character (Davies and Randle, 2001); only a few special cases have been examined e.g. (Su et al., 2003, Pyo and Kim, 2005). Third, some general boundaries (or very high Σ boundaries) have special properties based upon the rotation axis (Lejcek and Paidar, 2005), or "plane-matching boundaries", which are statistically more common than low Σ boundaries (Kawahara et al., 2005). Fourth, the benefit of low Σ or *special* boundaries has rarely been examined in non-cubic materials, even though the structure of low Σ boundaries is known (e.g. HCP – Wu et al., 2004, $L1_0$ – Singh and King, 1993). Much of the grain boundary engineering literature is more focused on creating low Σ boundaries with heat treatments than examining why they are effective.

While the CSL approach considers how well the lattices on either side of a boundary are aligned, another approach for assessing grain boundary character is based upon understanding the geometry of grain boundary dislocations (Brandon, 1966; Frary and Schuh, 2003). Bollmann (1982) developed the O-lattice approach to identify grain boundary dislocations, which has been used to explain diffraction contrast features in grain boundaries, (e.g. Solenthaler and Bollmann, 1986). Grain boundary dislocation Burgers vectors may or may not reside in the boundary plane, making them mobile or sessile, respectively. Even if boundary dislocations are mobile, they will face barriers at triple lines (where three boundaries meet), where they may or may not be able to continue to propagate, depending on whether the triple line is hard or soft (Fedorov et al., 2003). Triple lines are often described as I- or U-lines (Bollmann, 1984, 1988, 1991), where I-lines are typically intersections of Σ boundaries. I-lines do not have dislocations entering the boundary from adjacent grains, whereas U-lines do, resulting in disclinations, where crystal dislocations terminate along the triple lines. Dislocation transmission is possible through I-lines without development of dislocation debris, so they allow slip transfer. From this paradigm, triple line characteristics affect properties (Bollmann, 1991; Randle, 1995), including the likelihood of triple junction cracking (Wu, 1997; Wu and He, 1999). U-lines have higher energy (due to unbalanced dislocation content), providing sources or sinks for lattice dislocations during deformation, and are more susceptible to cavitation damage than I-lines.

There is a possible disconnect between the slip transparency of I-lines (junctions of low Σ boundaries), and the sense of boundaries being strengthening elements that resist dislocation motion (Tsurekawa et al., 1999; Kobayashi et al., 2005; Lim and Raj, 1985). Clearly, the influence of low Σ or *special* boundaries and associated I-lines on damage nucleation mechanisms is only partially understood. More importantly, the random boundaries that are more likely to develop damage nucleation need focused and systematic attention in order to identify how damage develops, because there will normally be a significant number of random boundaries in polycrystals.

1.3. Deformation transfer across grain boundaries

From the prior section it is clear that a good understanding of how deformation systems interact with boundaries is necessary before deformation transfer mechanisms can be distinguished from damage nucleation mechanisms. Three types of deformation transfer can be imagined near boundaries:

(1) the grain boundary acts as an impenetrable boundary that forces operation of additional in*tra*granular (self accommodating) slip systems that generate localized rotations (Zaefferer et al., 2003) in order to maintain boundary continuity;
(2) the boundary is not impenetrable, and slip in one grain can progress into the next grain with some degree of continuity (leaving residual boundary dislocations, and perhaps only partial ability to accommodate a shape change, as suggested in Fig. 1b);
(3) the boundary is transparent to dislocations, and (near) perfect transmission can occur, i.e. no deformation resistance (e.g. I-lines, low Σ boundaries (Lim and Raj, 1985) or low angle boundaries (Zaefferer et al., 2003; Kobayashi et al,. 2005)). This type is most typically modeled in an FEM mesh grain boundary.

Additionally, boundaries impose a threshold stress effect, such that strain bursts through a boundary occur with increasing stress/strain due to achieving a stress sufficient to activate a grain boundary source (Wang and Ngan, 2004; Hasnaoui et al., 2004; Kobayashi et al., 2005)). Also, the characteristics

of boundaries change with strain (Sun et al., 2000); e.g. the localized rotation gradients that reflect the geometrically necessary dislocations can change with increasing strain due to dislocation absorption or emission from the boundary that alters the boundary character. Furthermore, solute atom content can affect the activation energy for a dislocation source at a boundary (Floreen and Westbrook, 1969).

A number of studies have focused on boundary type (2), i.e. conditions where slip transfer is likely, but geometrically imperfect. Livingston and Chalmers (1957), who examined the geometry of slip transfer in bicrystals, concluded that deformation near boundaries required at least four activated slip systems within the two grains. Clark et al. (1992) and Lagow et al. (2001) determined that the slip transmission process often leaves residual dislocations in the boundary and requires a change in direction of the Burgers vector, along with a change in the plane orientation that results in two intersecting lines in the grain boundary plane. This geometry is illustrated in Fig. 2, and the three 'rules' that summarize conditions for slip transfer are:

1. The angle between the lines of intersection between the grain boundary and each slip system (θ) must be a minimum.
2. The magnitude of the Burgers vector of the dislocation left in the grain boundary must be a minimum.
3. The resolved shear stress on the outgoing slip system must be a maximum.

Based on these qualitative observations, quantitative geometrical expressions describing the likelihood of a slip transmission event have been developed. For example, Luster and Morris (1995) noted that large values of $\cos\psi \cos\kappa$, were correlated with observed instances of slip transmission, where ψ and κ are the angles between the slip plane normals or slip directions respectively of two slip systems on either side of a boundary. Ashmawi and Zikry (2003a) considered a slip transmission criteria based on the degree of *coplanarity* of slip systems engaged in deformation transfer that included both θ and ψ. Other instances of deformation transfer have focused more on Burgers vector *colinearity* ($\cos\kappa$ in Fig. 2), such as Gibson and Forwood (2002), who found that twin impingement at boundaries in TiAl is accommodated by á/2<110) ordinary dislocation slip on a variety of planes on both sides of the boundary, with residual dislocations left in the boundary. In a subsequent examination of equiaxed TiAl (Simkin et al. 2003a,b; Bieler et al. 2005c; Fallahi et al., 2006), slip transfer was examined in the context of the global stress state (discussed further in section II).

Computational modeling of dislocation-grain boundary interactions has been carried out at several length scales, from molecular dynamics (MD), to discrete dislocation dynamics (DD), to CP-FEM analyses. However, the experimental characterization necessary to validate modeling has not kept pace with the detail available with such simulations. While orientation imaging is valuable, it is only recently 3-dimensional (e.g. Spowart et al., 2003; Zaafarani et al., 2006; Konrad et al., 2006), and it lacks

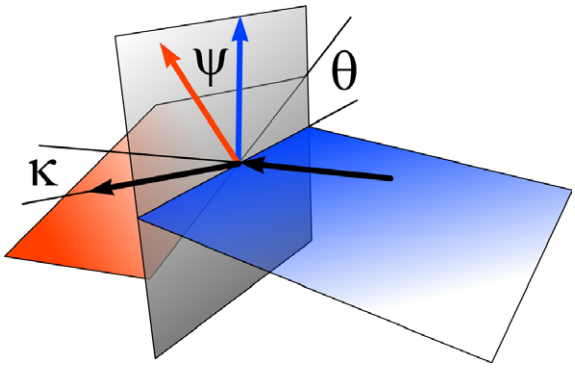

Fig. 2. Angles used to evaluate the geometry of strain transfer at a grain boundary. κ is the angle between slip directions, ψ is the angle between slip plane normal directions, and θ is the angle between traces of the slip planes on the grain boundary plane.

angular accuracy (~1° uncertainty in orientation). Consequently, there is an increasing effort to non-destructively obtain experimentally measured 3-D data sets (Juul-Jensen, 2005; Liu et al., 2005; Ice et al., 2005; Barabash et al., 2005; Shan and Gokhale, 2004), from which detailed computational models can be built. Quantitative experimental descriptions of dislocation activity near grain boundaries with known boundary conditions is possible using electron channeling contrast imaging (ECCI) methods (Simkin and Crimp, 1999; Simkin et al., 2003b).

Modeling and simulation of dislocation emission and interactions at the atomic scale has provided mechanistic insights (Yoo et al., 1995; Saraev and Schmauder, 2003; Hirth et al., 2006). Processes of dislocation nucleation from selected boundaries have been identified and described, and correlated with presence of particular polyhedral structural units (Spearot et al., 2005, 2007, 2008a; Spearot, 2008b; Tschopp et al., 2007, 2008; Brown and Mishin, 2007). Simulations have been able to identify mechanisms for grain boundary dislocation induced grain boundary motion (Cahn et al., 2006; Shen and Anderson, 2006). Dislocation absorption (slip transfer) has been modeled in $\Sigma 11$ boundaries (de Koning et al., 2002, 2003), which have confirmed the TEM observations of Clark et al. (1992) (above).

While simulations based upon discrete dislocations (DD) have focused more on crack propagation (e.g. Noronha and Farkas, 2004) or intragranular dislocation motion at an indenter tip (Miller et al., 2004), there are a few studies with grain boundaries using simple models (Espinosa et al., 2006; Balint et al., 2005; Cheong and Busso, 2004). It is possible to computationally combine atomistic simulations with dislocation dynamics modeling in a multi-scale approach (e.g. Noronha and Farkas, 2004; de Koning et al., 2003). While these simulations are insightful, for these methods to be reliable, they must be properly correlated with experimental observations.

At the microstructural scale, it is difficult to model deformation that takes place by dislocation absorption or transmission in boundaries (Ashmawi and Zikry, 2003a,b; Clayton and McDowell, 2004; Ma et al., 2006), as atomistic details that stimulate dislocation sources such as ledges (Fischer et al., 2003; Edwards et al., 2005) cannot be discretely modeled. Recent comparisons with characterized microstructures have shown that non-local formulations based on dislocation density evolution simulate experimentally measured local strains much better than formulations based upon phenomenological representations of strain hardening (indirect representation of evolving dislocation density) (Cheong and Busso, 2004, 2006; Rezvanian et al. 2006; Horstemeyer et al., 1999; McGinty and McDowell, 1999; Clayton and McDowell, 2003; Busso and Cailletaud, 2005; Ma et al., (2006a,b) Bardella, 2007). Special elements to handle dislocation accumulation and/or transmission through boundaries have been developed, but for practical reasons, they have finite thickness in the FEM mesh (Ma et al., 2006b; Ashmawi and Zikry, 2003a). However, there are few direct correlations between models and experiments with analysis sufficient to assess the model's ability to capture dislocation scale mechanistic interactions.

1.4. Damage nucleation at ambient temperature

Of the studies of heterogeneous deformation just described, the studies of Clayton and McDowell (2004); Ashmawi and Zikry (2003); Dunne et al. (2007); Cheong et al. (2007) sought ways to predict damage nucleation. Other recent studies have focused more on damage evolution, once it exists (e.g. Orsini and Zikry, 2001; Bennett and McDowell, 2002, 2003; Bjerken and Melin, 2004; Cao et al., 2005; Bieler et al., 2005a,b). Such studies show that the microstructure geometry has a large influence on void or crack growth once damage exists, but they offer no direct understanding about damage *nucleation* mechanisms.

An important and frequently used approach to model for void nucleation based upon cohesive interface energy was first presented by Needleman (1987) and Xu and Needleman (1994), who described the cohesive energy as an empirical scalar function that relates displacement with normal and shear traction evolution in the boundary. Such formulations have been adapted in damage nucleation models (Arata et al., 2002; Hao et al., 2003, 2004; Clayton and McDowell, 2004; Sfantos and Aliabadi, 2007; Kabir et al., 2007). Clayton and McDowell (2004) used non-local models to accurately predict local stress–strain history, and hence, tractions on the boundary. From this analysis, they identified a parameter that could be used to predict damage nucleation locations, based upon how much

accommodation by void damage is required by the material to deform to a given strain level. This model assumed isotropic interfacial energy for all boundaries (MD modeling can overcome this, but at a much smaller scale (Spearot et al., 2004, 2005, 2007, 2008a; Spearot, 2008). Cohesive interface energy models are appealing in that they are two dimensional, but they do not use the available information regarding operating slip systems to examine or analyze damage evolution.

Using a different approach, Ashmawi and Zikry (2003a,b) used the Clark et al. (1992) slip transfer criteria (quantified as $\cos\psi \cos\theta$) to correlate dislocation density with damage, based upon the assumptions that (1) damage develops with dislocation accumulation, and (2) that slip transfer mitigated dislocation accumulation. Because there is no reason to correlate concentrated dislocation activity with damage (concentrated dislocation activity could either mitigate or cause damage), this approach may not be effective. Ma et al. (2006a,b) also developed grain boundary elements that increase deformation resistance in boundaries and allow some slip transfer, but this has not been used to examine damage nucleation. There is clearly a need for an effective but simple way to identify how damage nucleates that takes into account the active slip system history in the vicinity of the boundary.

1.5. Assessment of current knowledge about damage nucleation

A summary of the state of knowledge about heterogeneous strain and damage nucleation can be provided as a list of hypotheses, starting with strain and slip system considerations, and continuing toward boundary structure considerations. Some of these are incompatible with each other, but they reflect this state of understanding/misunderstanding of damage nucleation, so they can guide experimental analysis and theoretical model development:

1. Damage nucleation always occurs at locations of maximum strain energy density (maximum area under *local* stress–strain curve).
2. Large local strains can provide geometric accommodation that can prevent damage nucleation.
3. Damage nucleation arises from slip interactions resulting from imperfect slip transfer through a boundary, which leaves residual dislocation content in the boundary plane.
4. Damage nucleation occurs in particular boundaries where unfavorable slip interactions take place at the boundary to weaken the boundary.
5. Slip interactions at the boundary are more (or less?) important than the magnitude of local strain for predicting damage nucleation.
6. Damage nucleation occurs in locations where there is maximum geometric incompatibility arising from highly activated slip systems that cause dominant shears in very different directions (e.g. Bieler et al., 2005b).
7. Damage nucleation is highly correlated with severe local strain heterogeneity, e.g. lattice rotations.
8. Dislocation density (non-local) formulations of crystal plasticity models are necessary to adequately predict the local strains, and hence the slip system activity needed to predict damage nucleation.
9. Damage nucleation probability is proportional to local hydrostatic tensile stress.
10. Damage nucleation depends upon cohesive strength of the boundary, i.e. Griffith criterion – energy needed to separate an existing interface.
11. Damage nucleation is more likely at triple lines than along boundaries, especially along U-lines.
12. Slip directions are more influential on damage nucleation than slip planes.
13. Low-Σ boundaries are less likely to accumulate damage than random boundaries.
14. Boundaries with low index crystal normals (facets) are more (or less?) likely to resist damage.
15. Twin boundaries resist damage because they repel dislocations from the boundary.
16. Twin boundaries resist damage because they allow efficient slip transfer.
17. Twin boundaries are schizophrenic (sometimes resistant, sometimes susceptible to damage nucleation).
18. Fatal flaws are located where there is the greatest density of local damage sites.
19. Fatal flaws are located where the size of nucleated damage grows the fastest.

2. New development of a slip system based definition of grain boundary strength

In contrast to high ductility metals such as pure copper, aluminum, and steel alloys damage nucleation is of crucial importance in low ductility metals and intermetallics, many of which are non-cubic. Such materials offer easier opportunities for analysis of active deformation systems, because they are fewer, and thus easier to analyze on the basis of microscopic evidence. Furthermore, an understanding of damage nucleation mechanisms is crucially important for technological applications in order to provide fundamental guidance to improve ductility and toughness.

Based on prior studies of microcrack nucleation in polycrystalline TiAl, there is uncertainty about whether detected acoustic signals arise from twinning or microcracks (Hu et al., 2006; Wu et al., 2006; Appel, 2005). Studies show that different microstructures result in different amounts of strain before acoustic signals are detected (detection of an acoustic event also depends on where the amplitude threshold is set). Another approach used to investigate damage nucleation using electron channeling contrast imaging methods showed that twinning and microcracking are intimately related, in that grain boundary microcracks are highly correlated with twin interactions. Unlike many metals, twinning is easily activated in TiAl (see crystal structure in Fig. 3). Ordinary dislocations operate on any given slip plane in a direction perpendicular to twinning vectors, so activation of both ordinary slip and twinning on the same plane is not usual. Superdislocations provide shears that have a c-component, but their activation is quite limited due to the large (high energy) Burgers vectors required to maintain crystal symmetry. Furthermore, the thickness of twins is an important correlative variable with microcracking, as illustrated in Fig. 4 (Ng et al., 2002). The microcracks present on the surface extend well beneath the surface, due to the geometry of the shear discontinuity, so the damage is not limited to the surface (Simkin et al., 2007). Because not all boundaries with significant twin interactions cracked, this material provides conditions where details of the boundary and deformation pro-

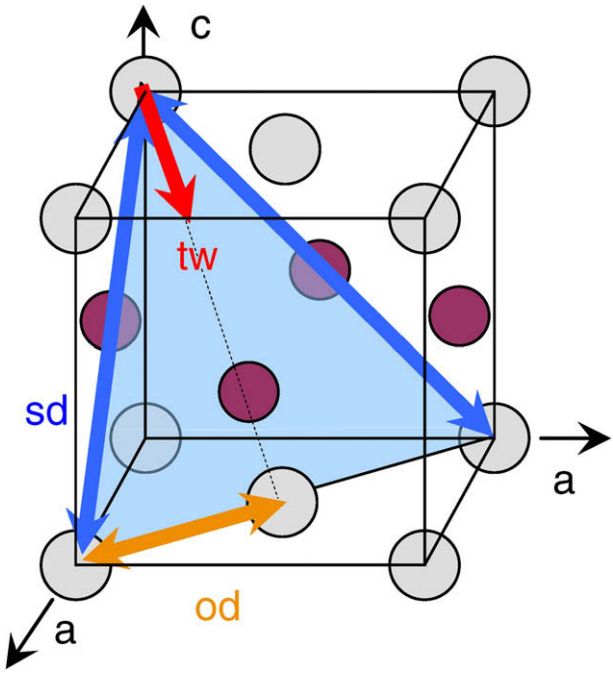

Fig. 3. $L1_0$ unit cell of TiAl, $c = 0.407$ nm, $a = 0.400$ nm, $c/a \sim 1.02$, twin (tw), ordinary dislocations (od) and superdislocations (sd) shown.

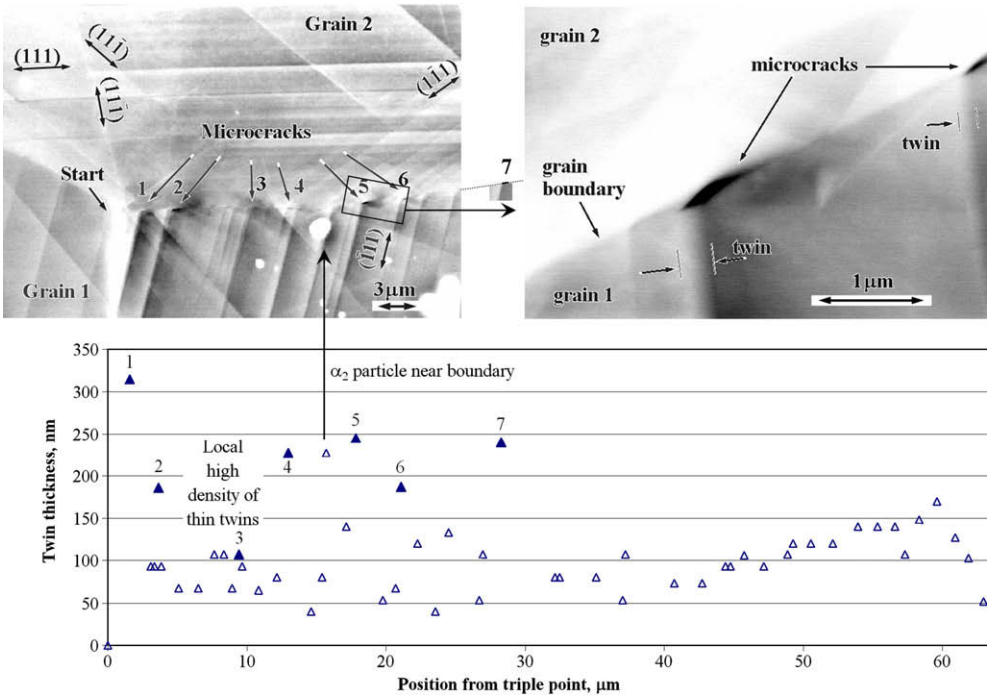

Fig. 4. Microcracks are correlated strongly with the thicker twins; exceptions occur when many thin twins are close together, or when α_2 particles alter local strain conditions. (adapted from Ng et al., 2002, Figs. 8–11).

cesses in its neighboring grains could be analyzed. Results of these investigations have led to definition of a slip based definition of grain boundary character.

2.1. Experimental assessment of damage nucleation

The experimental investigation used an electropolished 4-point bend specimen deformed to a surface plastic strain near 1.4% (Simkin et al., 2003a). A uniformly stressed region of ~6 mm^2 was examined near the center of the specimen, where about 20 microcracks were found. The majority of the cracks developed at grain boundaries between γ grains (a few cracks were in the interface between TiAl and Ti_3Al). Selected area channeling patterns (SACPs) were used to determine the absolute orientations (Simkin et al., 2003b) of about 50 grains in the neighborhood of 11 microcracks in γ–γ boundaries. Eleven intact boundaries with apparently similar geometrical character to the microcracked boundaries were also analyzed. The slip behavior near these 22 boundaries was examined using electron channeling contrast imaging (Simkin and Crimp 1999) to observe slip and twinning activity. Grain boundary normal directions were estimated from serial sectioning, indicating that all of the boundaries analyzed had at least 85% of the global tensile stress operating perpendicular to the boundary plane ($|\hat{\mathbf{n}}_{gb} \cdot \hat{\mathbf{t}}|$ in Table 1, where the geometry of a twin interacting with a grain boundary is indicated in Fig. 5).

2.2. Fracture initiation parameter defined

Slip transfer parameters such as those defined by Luster and Morris (1995), or Ashmawi and Zikry (2003a) show no correlation with the presence of microcracks (Crimp et al., 2003), so a different approach was taken. Instead of a single geometrical parameter, a multiplicative figure of merit (to

Table 1
Statistical characteristics of components and of fracture initiation parameter products

	max m	$\lvert\hat{\mathbf{n}}_{gb}\cdot\hat{t}\rvert$	$\lvert\hat{\mathbf{n}}_{sp}\cdot\hat{t}\rvert$	$\lvert\hat{\mathbf{b}}_{tw}\cdot\hat{\mathbf{n}}_{gb}\rvert$	$\lvert\hat{\mathbf{b}}_{tw}\cdot\hat{t}\rvert$	Σ term	F_1	F_4	F_7	F_8	F_9
Cracked											
Mean	0.423	0.902	0.573	0.717	0.767	3.428	1.100	0.994	2.057	5.841	0.482
Std	0.070	0.061	0.165	0.203	0.113	0.495	0.232	0.220	0.668	1.393	0.367
Intact											
Mean	0.423	0.892	0.647	0.605	0.671	3.037	0.844	0.753	1.403	4.33	0.845
Std	0.072	0.124	0.144	0.234	0.109	0.678	0.222	0.236	0.572	1.32	0.498
% Diff from cracked	0.0	1.1	−12.9	15.6	12.5	11.4	23.3	24.2	31.8	25.9	−75.2
t-Test[a] $1-\alpha$	0.47%	24.7%	72.2%	75.3%	**94.4%**	86.1%	**98.5%**	**97.7%**	**97.7%**	**98.3%**	**93.3%**
Statistic[b]	<<90%	<<90%	<<90%	<95%	~**95%**	<95%	**98%**	**98%**	**97.5%**	–	–

[a] Student t-distribution based hypothesis tests on comparative means were conducted using Excel™ (assuming unequal variances, normal distributions with two tails).
[b] The Mann–Whitney statistic is used, which is suitable for small populations.

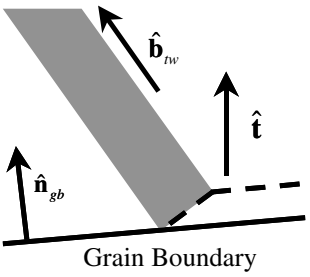

Fig. 5. Mode I opening strain at grain boundary due to twin (dashed line).

correlate with the probability of nucleation of a microcrack) based on several geometrical factors that could influence microcracking was explored, resulting in a phenomenological *fracture initiation parameter* (*fip*):

$$F_1 = m_{tw}|\hat{\mathbf{b}}_{tw}\cdot\hat{\mathbf{t}}|\sum_{ord}|\hat{\mathbf{b}}_{tw}\cdot\hat{\mathbf{b}}_{ord}| \tag{1}$$

Variations of this idea are presented in equations as F_i, where i is a label (Simkin et al., 2003a,b; Ng et al., 2005; Bieler et al., 2005c). The *fip* parameter F_1 is the product of three terms. The first term is the Schmid factor of the most highly stressed twinning system in a grain pair, m_{tw}, which identifies twins that cause the largest shear discontinuity at a grain boundary. The second term is the scalar product of the unit vector of this twin's Burgers vector direction, $\hat{\mathbf{b}}_{tw}$, and the maximum tensile stress direction $\hat{\mathbf{t}}$, i.e. $\hat{\mathbf{b}}_{tw}\cdot\hat{\mathbf{t}}$, which identifies the strength of a mode I opening component at the boundary. The third term is the sum of scalar products between the Burgers vector of the same highly stressed twin system and the Burgers vector of ordinary dislocation systems in both grains, describing how well the twin shear can be accommodated by dislocation activity. The ^ denotes *unit* vectors, so that only the directional component of the scalar products are evaluated. The $\hat{\mathbf{b}}_{tw}$ refers to Burgers vector of the twin system with the highest value of the Schmid factor m_{tw} in the *initiating* grain, and the most important contribution to the summation takes place over the slip systems in the *responding* grain. Table 1 shows that there is 98% confidence that the mean value of F_1 for the 11 cracked boundaries is larger than the mean of the 11 intact boundaries (which have similar geometrical microstructural arrangements). Note that the mean and standard deviation of the maximum Schmid factors m_{tw} are the same, and the grain boundary normal directions are similarly aligned with the tensile axis.

A subtle but important point is that the sum term will be largest for misorientations where there are more than one slip system with sub-optimal slip transfer conditions (near-perfect slip transfer will

have a smaller value). Thus the sum term can identify the class of boundaries where there is the greatest likelihood of leaving residual dislocation segments in the boundary, as described above in Section 3.

A number of variations of this *fip* parameter were evaluated using the student t-test as well as a nonparametric statistical analysis suitable for small populations (Fallahi et al., 2006; Kumar et al., 2008).[2] The confidence level shown in Table 1 is used as a figure of merit for evaluating whether a particular *fip* variation expresses information present in the experimental data set in a physically meaningful way. For example, a variation identified as F_4 includes the orientation of the grain boundary normal (estimated from serial sectioning).

$$F_4 = m_{tw}|\hat{\mathbf{b}}_{tw}\cdot\hat{\mathbf{t}}||\hat{\mathbf{n}}_{gb}\cdot\hat{\mathbf{t}}|\sum_{ord}|\hat{\mathbf{b}}_{tw}\cdot\hat{\mathbf{b}}_{ord}| \tag{2}$$

Including the grain boundary normal information (Eq. 2) showed no statistical improvement over F_1, indicating that the grain boundary normal is not very important (for the sampled population of boundaries that were approximately perpendicular to the tensile axis). Furthermore, nearly the same statistical confidence can be achieved for a simpler expression in Eq. 3:

$$F_7 = |\hat{\mathbf{b}}_{tw}\cdot\hat{\mathbf{t}}|^2\sum_{ord}|\hat{\mathbf{b}}_{tw}\cdot\hat{\mathbf{b}}_{ord}| \tag{3}$$

Eq. 3 recognizes that $|\hat{\mathbf{b}}_{tw}\cdot\hat{\mathbf{t}}|$ is already present in m_{tw}, which also includes $|\hat{\mathbf{n}}_{sp}\cdot\hat{\mathbf{t}}|$ where $\hat{\mathbf{n}}_{sp}$ is the slip plane normal (hence, $F_7 = F_1/|\hat{\mathbf{n}}_{sp}\cdot\hat{\mathbf{t}}|$). This suggests that the slip plane offers no insight or meaning in the process of damage nucleation; in fact, the values of $|\hat{\mathbf{n}}_{sp}\cdot\hat{\mathbf{t}}|$ are larger for intact boundaries, contrary to other components. Thus, neither the slip plane orientation nor the orientation of the grain boundary contributes significant information to the *damage nucleation process*, whereas the slip plane and the grain boundary normal are considered important in much of the literature regarding *slip transfer*.

2.3. Some enhancements to the fracture initiation parameter

Further exploration of this approach identified three other factors that could enhance the separation between intact and cracked populations (details and statistics are presented in Kumar et al. (2008)). Fig. 6 depicts how F_1 can be represented in an idealized manner using a Gaussian curve (the populations identified in the work to date are not always Gaussian), and compares it with the ratio of the elastic stiffness along the tensile direction between the two grains. The degree of overlap in the intact and fractured populations is larger for the elastic modulus effect, but the elastic component of the deformation near the boundary could also influence crack nucleation, because a greater compliance in one grain can help accommodate strain incompatibilities.

Next, Eq. 4 describes a method by which the orientation of the slip plane traces in the grain boundary plane ($\cos\theta$ in Fig. 2) can contribute to distinguishing between the cracked and intact populations.

$$F_8 = m_{tw}|\hat{\mathbf{b}}_{tw}\cdot\hat{\mathbf{t}}|\sum_{ord}|\hat{\mathbf{b}}_{tw}\cdot\hat{\mathbf{b}}_{ord}|\sum_{ord}|\hat{\mathbf{n}}_{tr,tw}\cdot\hat{\mathbf{n}}_{tr,ord}| \tag{4}$$

However, the effect of the second sum term is statistically weaker than the Burgers vector sum term, but it does increase the confidence for separating populations slightly. Also, Eq. 5 is based upon the orientation of the basal plane in the neighboring grain as defined by the basal plane normal, $\hat{\mathbf{c}}$, rather than specific ordinary slip directions.

$$F_9 = |\hat{\mathbf{b}}_{tw}\cdot\hat{\mathbf{t}}|/|\hat{\mathbf{b}}_{tw}\cdot\hat{\mathbf{c}}| \tag{5}$$

F_9 is also able to distinguish between the intact and cracked populations with a statistic that is similar to F_1 (Kumar et al., 2008). F_9 is large when $|\hat{\mathbf{b}}_{tw}\cdot\hat{\mathbf{c}}|$ is small, implying that ordinary dislocation directions are close to being perpendicular to the dominant twinning Burgers vector. This is a way of saying that it is difficult to convert a twinning Burgers vector in one grain into a shear displacement involving

[2] As discussed in [Kumar et al. 2008], the standard t-test gives equivalent confidence as the Mann-Whitney statistic.

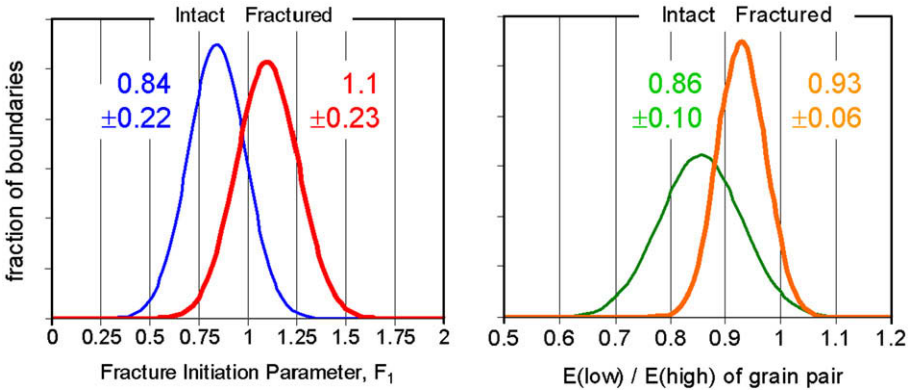

Fig. 6. Gaussian depictions of intact and fractured populations based upon a plastic deformation process using fip F_1, and an elastic modulus ratio of the two neighboring grains ($E(C_{ijkl})$ from He et al., 1997; Nye, 1955a, 1955b).

an ordinary slip direction on *any* slip plane. This, along with the lack of sensitivity to slip plane orientations in all of the above, is consistent with TEM observations of Gibson and Forwood (2002), who observed ordinary dislocations accommodating twin shears at boundaries where the dislocations are present on a number of different planes. There are probably additional ways to examine factors based upon elastic and plastic deformation details that could offer further insight on the mechanisms of damage nucleation.

2.4. Application to crack propagation

This *fip* approach was also used to examine crack propagation using a notched 4-point bending specimen geometry shown in Fig. 7a (Ng et al., 2005). A specimen with an arrested crack was analyzed similarly as described above, and the microstructure ahead of the crack tip was characterized to identify weak and strong boundaries using a directional *fracture propagation parameter* (*fpp*), appropriate for deformation from grain A toward grain B.

$$F_{A\to B} = m_{tw}|\hat{\mathbf{b}}_{tw-A}\cdot\hat{\mathbf{t}}|\left(\sum_{ord-B}|\hat{\mathbf{b}}_{tw-A}\cdot\hat{\mathbf{b}}_{ord-B}| + \sum_{tw-B}|\hat{\mathbf{b}}_{tw-A}\cdot\hat{\mathbf{b}}_{tw-B}|_{if>0}\right) \tag{6}$$

This *fpp* differs from the *fip* in that twins in grain A may be accommodated by twins in addition to ordinary dislocations in grain B. For this experiment, methods to speed up measurement of the true orientation of grains were used so that about 40 cracked and intact boundaries were analyzed, which provided a more convincing representation of the ability of the *fpp* to differentiate between intact and cracked boundaries, as illustrated in the histogram in Fig. 7b. Further deformation of the specimen resulted in the crack following the path defined by the highest density of weak boundaries (Ng et al., 2005).

The probabilistic approach in the *fip* has been shown to be effective in separating strong and weak boundaries in both crack nucleation and in crack propagation experiments. In contrast to slip transfer parameters, which are often dominated by considerations of the degree of slip plane coplanarity, interactions of slip directions appear to be more important when considering grain boundary damage nucleation. This result is also consistent with a recent study of fatigued Cu bicrystals using electron channeling contrast, where the slip direction of dislocation pileups (which depend on the slip system with the highest Schmid factor) was identified to be more significant in nucleating fatigue cracks than slip planes, grain boundary plane normals, or grain boundary character (Zhang and Wang, 2003). This corroboration suggests that a slip vector based (rather than slip plane based) metric may provide a robust method to predict locations of damage nucleation.

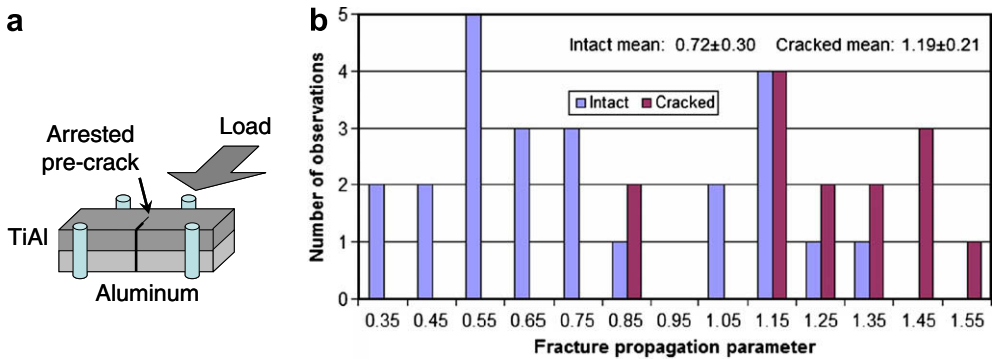

Fig. 7. (a) Geometry of crack growth experiment, and (b) Fracture propagation parameter (Eq. 6) is able to separate intact and cracked populations effectively.

2.5. Grain boundary character

To assess whether the boundary strength as identified by the *fip* is correlated with established measures of grain boundary character, the angle–axis relationships between the set of 22 boundaries were assessed using the cubic definitions for Σ boundaries. In addition, the same information can be used to describe the degree of twist in the misorientation. These results are plotted in Fig. 8, which shows that there were as many cracked as intact boundaries having Σ character. With regard to structure used to describe *special* boundaries, there were more cracked boundaries with mixed twist-tilt character than intact boundaries, and cracked Σ boundaries had a higher degree of twist, suggesting that boundary structure may play a more significant role than CSL description (Randle, 2001). Thus, there is no obvious correlation between energy based descriptions of grain boundary character in cubic metals, and the strength of a boundary as described by the effect of deformation system interactions (*fip*).

3. Crystal plasticity-finite element modeling of microstructures with damage nucleation

Because the variables used for evaluating the *fip* are naturally computed in CP-FEM modeling of microstructures, it is possible to evaluate the *fip* in the CP-FEM setting. Furthermore, a CP-FEM

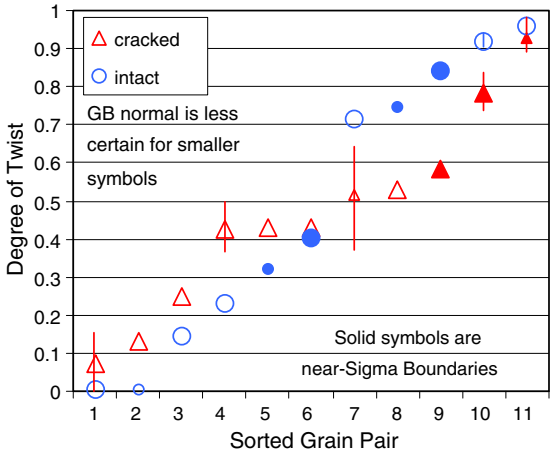

Fig. 8. Grain boundary character of intact and cracked boundaries show no obvious correlations with cracking. Selected datum points show magnitude of uncertainty in measurement. Adapted from Kumar et al. (2008), Fig. 7, with permission from ASME.

analysis provides local stresses and strains that are not easily measured experimentally (strains and rotations *can* be partially assessed using differential image correlation and OIM data to track rotations and orientation gradients).

3.1. Mesh, boundary conditions, and constitutive model

A quasi-3-D mesh based upon the highly characterized microstructure in Fig. 9 is shown in Fig. 10. The microcracks in Fig. 9 differed from all other cracked boundaries, in that the microcracks were associated with the twin system in the grain pair with the third highest – rather than the highest – Schmid factor (Simkin et al., 2007), making this microstructure especially desirable to analyze. The mesh was built by making a 2-D mesh where nodes of elements in each grain matched spatially at the boundary (simulating type 3 transparent boundaries in Section 3 – hence there was no attempt to model grain boundary dislocations or dislocation transfer through a boundary). The model was made 3-dimensional by expanding it into a 5-element thick stack with about 8000 elements, such that the grain boundaries were all perpendicular to the surface. Each element had eight integration points. The modeled microstructure was surrounded by a rim of CP elements to provide constraint that represents the surrounding microstructure. The Bunge Euler angles chosen for this surrounding material were ϕ_1,Φ, φ_2 = 90°,90°,0°, an orientation that provided symmetrical slip behavior with respect to the loading direction. This orientation is slightly softer than average, but it imposed considerable resistance to *yz* or *yx* shear along the vertical boundaries of the modeled microstructure. Boundary condi-

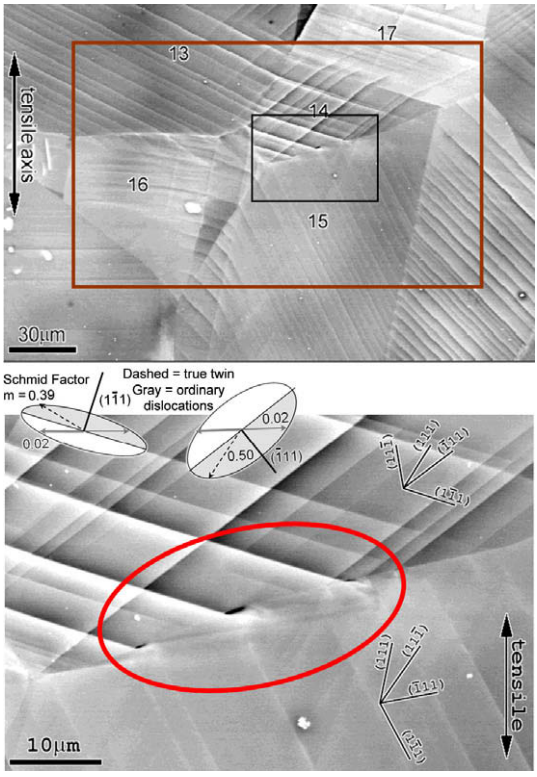

Fig. 9. Electron Channeling Contrast Image (ECCI) of microcracks formed between grains 14 and 15, while boundaries between grains 13 and 16, and between 14 and 17 (an annealing twin) remained intact after a surface strain of about 1.4%. The microstructure within the larger box in the upper figure was modeled with a FEM mesh; the smaller box is enlarged to show three microcracks correlated with twin intersections.

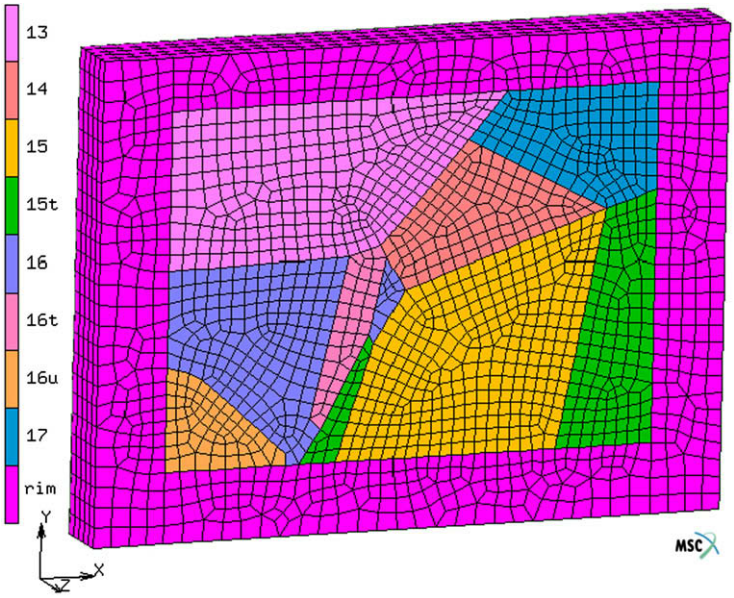

Fig. 10. Quasi-3-D model of grains in Fig. 9.

tions were imposed with zero vertical displacement on the bottom edge and a tensile face load on the top edge, with the front and back surfaces being unconstrained.[3] The laboratory coordinate system is indicated in Fig. 10.

The constitutive description of the material is based on a crystal plasticity formulation using the multiplicative decomposition of the total deformation gradient and taking into account the anisotropic elastic constants (Kalidindi et al., 1992; Kalidindi and Anand, 1993; Raabe et al., 2001; Sachtleber et al., 2002). Both dislocation slip and mechanical twinning are incorporated as bidirectional and unidirectional deformation systems, respectively. Hence, mechanical twinning operates in a diffuse manner similar to slip, unlike the intense shear confined between discretely spaced planes that are apparent in the micrographs (Figs. 4 and 8).

The deformation kinetics, expressed as the total plastic velocity gradient L_p, are written as

$$L_p = \sum_{\alpha}^{N_{slip}} S^{\alpha}\dot{\gamma}_{0,slip}\left|\frac{\tau^{\alpha}}{\tau_c^{\alpha}}\right|^n \mathrm{sgn}(\tau^{\alpha}) + \sum_{\beta}^{N_{twin}} S^{\beta}\dot{\gamma}_{0,twin}\left|\frac{\tau^{\beta}}{\tau_c^{\beta}}\right|^n H(\tau^{\beta}) \tag{7}$$

[3] Notes on boundary conditions and meshes: In simulations using a simpler (FCC-like) material model, each rim element contained 4 random crystal orientations; while this obviously altered the deformation details in elements near the rim, the deformation patterns more than a few elements from the rim were essentially the same as when a single orientation with a moderate plastic property was chosen (the latter was also convenient). The thickness of 5 elements was chosen to have a sufficient number to identify 3-D interactions between grain shape and plastic anisotropy. A more correctly represented 3-D mesh containing 28,000 elements was also constructed with 8 elements thick, using grain boundary and annealing twin inclinations based upon information gained from serial sectioning of the physical specimen. This 3-D mesh provided results similar to the quasi-2-D mesh when using a standard FCC crystal slip system, but with the TiAl slip system, the mesh was less stable, probably because this 3-D mesh had some elements that were much less equiaxed. The deformation patterns in the 3-D mesh were somewhat different where the modeled grain geometry was significantly different, but up to the point where it became unstable at ~0.5% plastic strain, the overall patterns of stress and deformation were the same as shown in the quasi-3-D (2-D projected) mesh. ***In particular, the deformation history where the cracks were observed was nearly the same.*** Other boundary condition explorations included constraining back plane nodes for zero out-of-plane displacement; while this altered the stress-strain history, it did so uniformly such that the overall pattern of stress and strain was similar.

with $\dot{\gamma}_{0,\mathrm{slip}} = \dot{\gamma}_{0,\mathrm{twin}} = 10^{-3}$ s^{-1} as reference shear rates, $n = 20$ constant stress exponent, S^α and S^β the Schmid matrices with respect to the unstrained reference state, τ^α and τ^β the resolved shear stress on slip and twin system α and β. τ_c^α and τ_c^β are the slipping and twinning resistances, and H is the Heaviside step function. The evolution of τ_c^i, where $i = 1, 2, ..., 16$ iterates thru the three slip system families noted in Table 2, is formulated in a phenomenological manner:

$$\mathrm{d}\tau_c^i = \sum_{\xi}^{N_{\mathrm{slip}}} h_{0,\mathrm{slip}}^{\xi}\left(1-\frac{\tau_c^{\xi}}{\tau_s^{\xi}}\right)^{a_\xi}[q+(1-q)\delta_{i\xi}]\mathrm{d}\gamma_\xi + \sum_{\zeta}^{N_{\mathrm{twin}}} h_{0,\mathrm{twin}}\left(1-\frac{\tau_c^{\zeta}}{\tau_s}\right)^{a}[q+(1-q)\delta_{i\zeta}]\mathrm{d}\gamma_\zeta \tag{8}$$

with δ being 1 if the two involved systems are coplanar and 0 otherwise. The hardening parameters, $h_{0,\mathrm{slip}}^{\xi}$, $h_{0,\mathrm{twin}}$, τ_s^{ξ}, τ_s, a_ξ, a and q as well as the initial resistances $\tau_{0,c}$ are listed in Table 2. The parameters for ordinary dislocations were determined by fitting to the stress–strain data of the same batch of material (Knaul et al., 1999). As twinning is known to be as easy as ordinary slip, if not easier (Mahapatra et al., 1995), parameters were chosen to provide a lower yield stress and a lower hardening rate. The superdislocation parameters were chosen to be about three times as strong as ordinary dislocations. These choices provide a reasonable estimate for the likely behavior of the TiAl alloy used, but the parameters have not been adjusted using any type of optimization process. This material model was implemented as a user material of type HYPELA2 into the commercial FEM package MARC.

3.2. Simulated deformation

Upon simulated loading to ~1.8% engineering plastic strain, Fig. 11 shows the von Mises stress (left side) and the equivalent total strain (right side) in the model on the front (top plots) and back faces (bottom plots). In Fig. 11, most of the grain boundaries (identified with white lines) developed large stresses, but not in a uniform manner. These patterns of stress and strain were similar on the front and back side, but larger on the back side, despite the fact that the geometry was the same, due to interactions between grain shape and plastic anisotropy with respect to the tensile axis. Also, the patterns of σ_{yy} or ε_{yy} were nearly the same as the Mises stress or equivalent strain (but lower in magnitude) indicating that the tensile stress state dominated (white arrows indicate regions where the von Mises or equivalent strain differed significantly from σ_{yy} or ε_{yy}). The principal strain directions in most elements were tilted no more than ~10° from the idealized uniaxial deformation direction. These observations indicate that despite the heterogeneous stress and strain states, uniaxial tension dominated the deformation process.

The pattern of stress visible in Fig. 11 is similar to the pattern that arose primarily from elastic anisotropy just as plastic slip began to occur, as the pattern of stress only changed in magnitude from the time when strains just began to develop, up to the value shown (though not proportionally). To evaluate the effect of elastic properties on the evolution of stress and strain, the elastic constants were changed from isotropy (similar to W) to highly anisotropic properties (similar to Pb), while maintaining the same plastic properties. While the pattern of stress at the yield point varied according to the anisotropy, after about 1% strain, the stress and strain field gradients were similar regardless of the elastic properties. This implies that the combination of grain geometry and slip processes arising from the crystal orientation is much more significant than elastic anisotropy. This outcome is consistent with a stochastic study by Zeghad et al. (2007).

The variance of local stress and strain is consistent with experimental observations. Variations in slip trace density (spacing) are apparent in Fig. 9, which are mostly from twins, but dislocation slip bands are also evident in grains 16 and 17, where ordinary dislocation slip had a high Schmid factor

Table 2
Hardening parameters used to describe evolution of the CRSS

Slip or Twin system (#)	{*hkl*}⟨*uvw*]	$\tau_{0,c}$, MPa	τ_s, MPa	h_0, MPa	a	q
True twin Eq. 4	{111}⟨112]	50	130	5500	1.5	1.4
Ordinary dislocation Eq. 4	{111}⟨110]	60	130	22000	1.5	1.4
Super dislocation Eq. 8	{111}⟨011]	180	300	19000	2	1.4

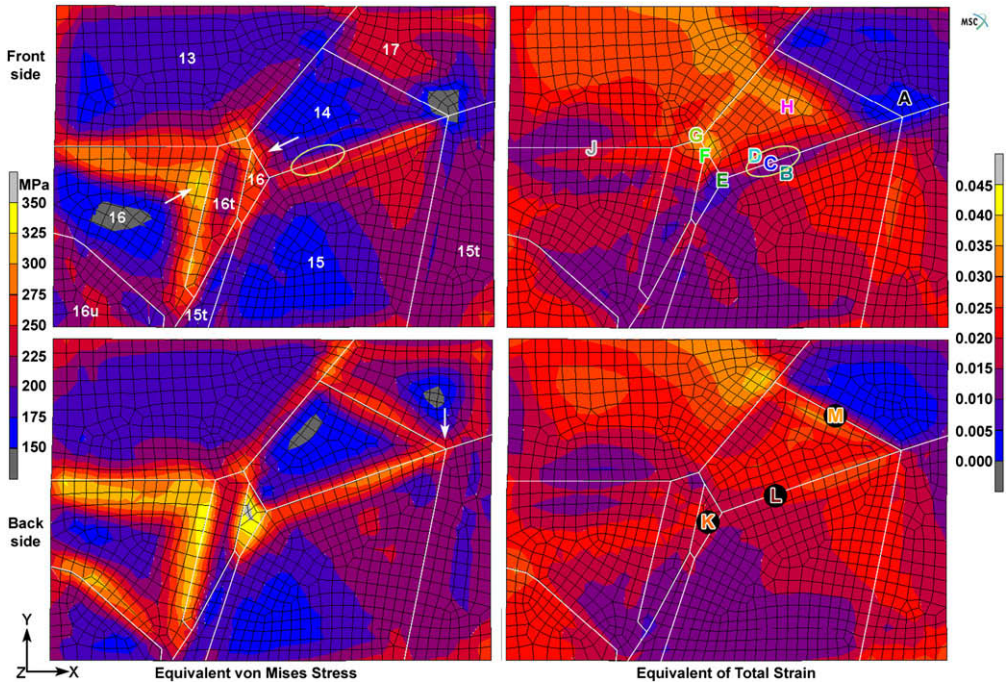

Fig. 11. Interior of the FEM model (rim was removed) illustrating the distribution of equivalent stress and strain in the microstructure. White lines indicate grain boundaries in the model, and the ellipses indicate the location of microcracks in the experiment. White arrows indicate the only locations where the stress tensor had significant non-*yy* components; the magnitude of the σ_{yy} stress and ε_{yy} strain was uniformly similar to the equivalent strain.

(slip bands are typically less distinct than twins). In general, the strains are more evenly spread than the stresses, and the locations of high and low total strain are not directly related to the stress. The relationships are much more complex, and affected by deformation in neighboring grains; indeed the band of high strain from upper left to lower right could not be visually inferred from the stress state. As the von Mises stress is a scalar measure of elastic strain energy, it would be natural to expect damage nucleation to develop where the von Mises stress is high. Interestingly, neither the maximum von Mises stress nor equivalent strain is found in the vicinity where microcrack nucleation was observed (marked by ellipse).

In the region of the microcracks, there is a notable strain gradient, but the magnitudes of the stress and strain are moderate, as indicated in Fig. 12, which shows local stress–strain histories at lettered locations indicated in Fig. 11. Locations of extremely low and high values of stress and strain provide bounds on the range of stress–strain histories in the material. Several nodes along the top of the annealing twin of grain 16 (thin green curves F and G in Fig. 12) show moderate stress–large strain histories that reflect the local strain concentration. Compared to points F and G, the stress–strain histories where the microcracks were observed show less strain (labeled C in Fig. 11, and plotted with a heavy blue dotted line in Fig. 12; nodes B and D, below and above the microcracked boundary have solid blue lines). The strain energy (area under the local stress–strain curve) at the crack location is significantly smaller than at points K, F, G, L, M, or H. The strain on the back side (node L) near the microcracks is much larger than on the front side.[4] It is remarkable that microcracks developed where neither the stress nor the strain was large, indicating that a high strain energy did not cause fracture.

[4] Following from prior footnote, the true 3-D mesh had local stress strain curves that were different in details, but overall, similar relative histories in similar places.

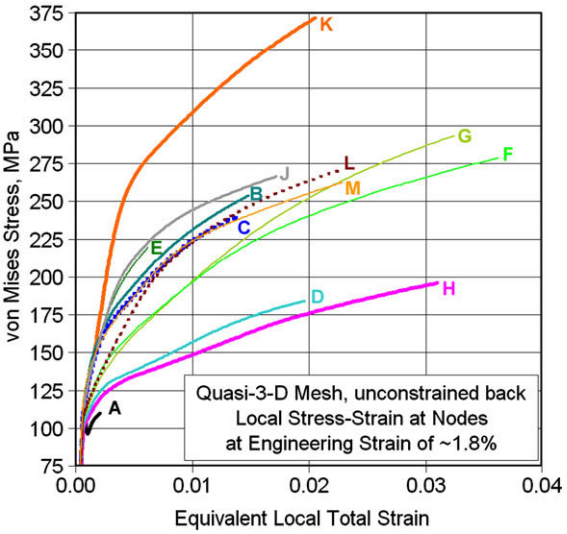

Fig. 12. Local stress–strain history of nodes in extreme locations in the model, near the grain 16 twin (green), and near the observed microcrack (blue) (For interpretation of colour mentioned in this figure, the reader is referred to the web version of this article.).

The strains and strain *gradients* (Fig. 11 right side) are maximized *near*, but not at the observed location of the microcracks; a local strain maximum occurred at a location along a different boundary 5–10 elements away from the actual crack nucleation sites. This suggests that large local strains in the real material may have occurred near points F and G to accommodate strain incompatibilities and hence prevent damage, but the accommodation of this strain concentration led to the need to transmit strain across a nearby weak boundary (the 14–15 boundary). The largest microcrack in Fig. 9 is correlated with a twin that points to (and possibly originated from) the triple point at the top of grain 16-twin.

The lack of correlation between high local strain energy and the location of damage nucleation indicates that another predictive approach is needed. Thus, a strain concentration may be, at best, a pointer to a neighborhood where damage could nucleate, if there is a combination of grain orientations, slip activity, and boundary misorientation that cause a nearby boundary to become weak. The fracture initiation parameter analysis described above, which is based on slip vectors, and hence shears on particular slip systems, is considered next.

3.3. Evaluation of shears on slip and twinning systems

The shear rate on the most active slip systems in elements near the microcrack locations (nodes B, C, and D) in grains 14 and 15 are plotted in Fig. 13 (several slip systems are illustrated with tilted unit circles and plane normals to assist in visualizing their operation). On the front side in grain 14, only two twin systems are active (green and purple curves in the upper left plot). Up to about 0.5% engineering strain, a greater shear occurs on the twin system with the larger Schmid factor (purple curve), as expected from the global stress. After about 0.5% strain, the shear on the twin system with a lower global Schmid factor (green curve) accelerates considerably, presumably due to the need to maintain boundary compatibility, eventually contributing more shear to the total strain than the system with the highest global Schmid factor. It is clear that near the boundary on the front side, shear was preferred on this 3rd highest system, but this system was not active on the back side. There are significant differences in the distribution of shear on different slip systems in the front and back of grain 15 as well, but the amount of the shear accomplished on the most highly stressed twin system in grain 15 is not quite as great as that in grain 14. This result can be further understood in the spatial variation

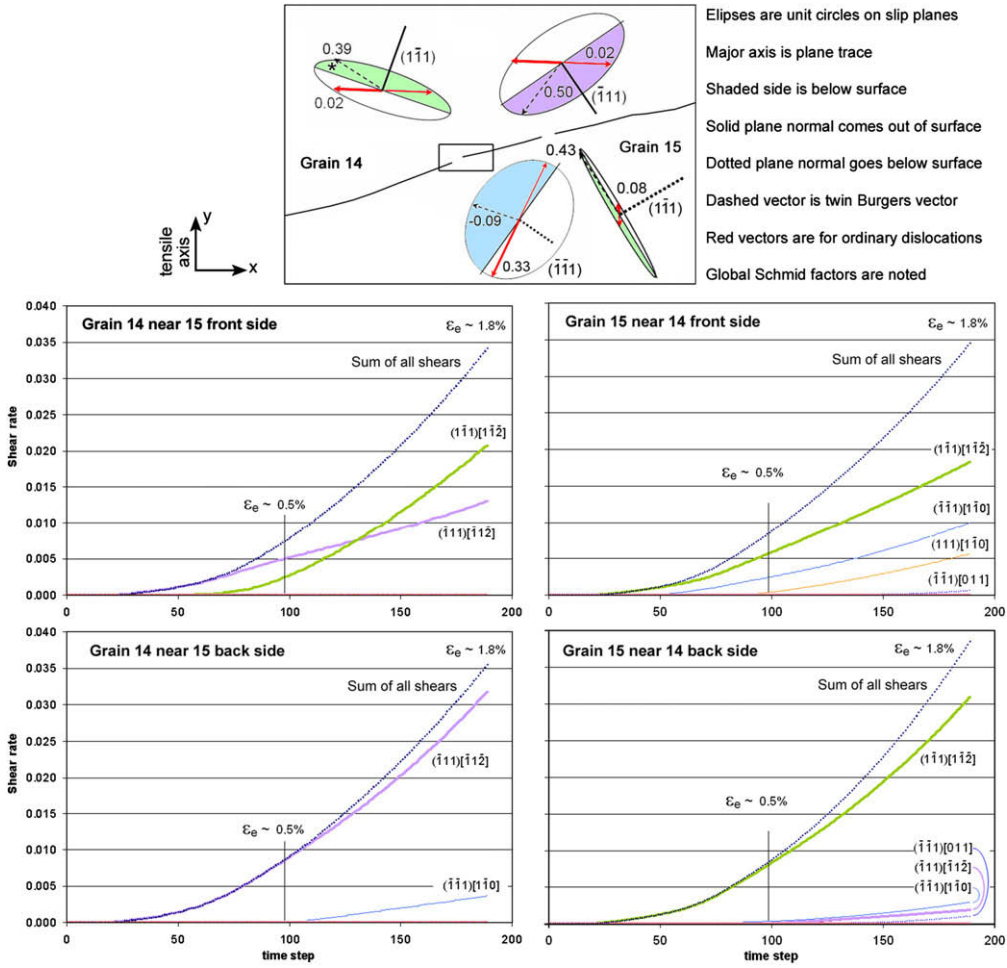

Fig. 13. Shear rates on slip systems on the front (nodes B and D) and back sides near the 14–15 grain boundary microcracks.

of the shear rates shown in Fig. 14, where the *local generalized* Schmid factor (based on the stress tensor) for the twin system responsible for the cracks had the highest value in either grain at the location where microcracks developed. Clearly, the greater amount of shear in the grain 14 elements next to the boundary is supported by a locally high Schmid factor. The stress state at the boundary is quite different from the grain interiors, though still dominated by uniaxial tension. This result shows that the damage nucleation rule identified experimentally is valid locally, making this unusual microcracked microstructure consistent with the rest of the microcracked boundaries. Clearly, it is important to obtain the local stress–strain history to evaluate the *fip* most effectively.

Further inspection of Fig. 14 shows that the CP-FEM model cannot simulate the highly planar shear evident in the SEM images in Fig. 9, where twins propagated all the way across grain 14 to connect regions of high activity in the CP-FEM model. Observed twins are symbolically overlaid on the FEM mesh to show how they connect regions of high activity through the middle of the grain. The same phenomenon occurred in grain 13, where the lower Schmid factor twin system (green) showed much more activity in the SEM ECCI image in Fig. 9 than the (-111) twin system (purple). The CP-FEM model provides information about where twin shear is likely in a given grain, but not the spatial details of the contiguous planar shear that goes with twinning. Thus, it is possible to predict regions of higher twin

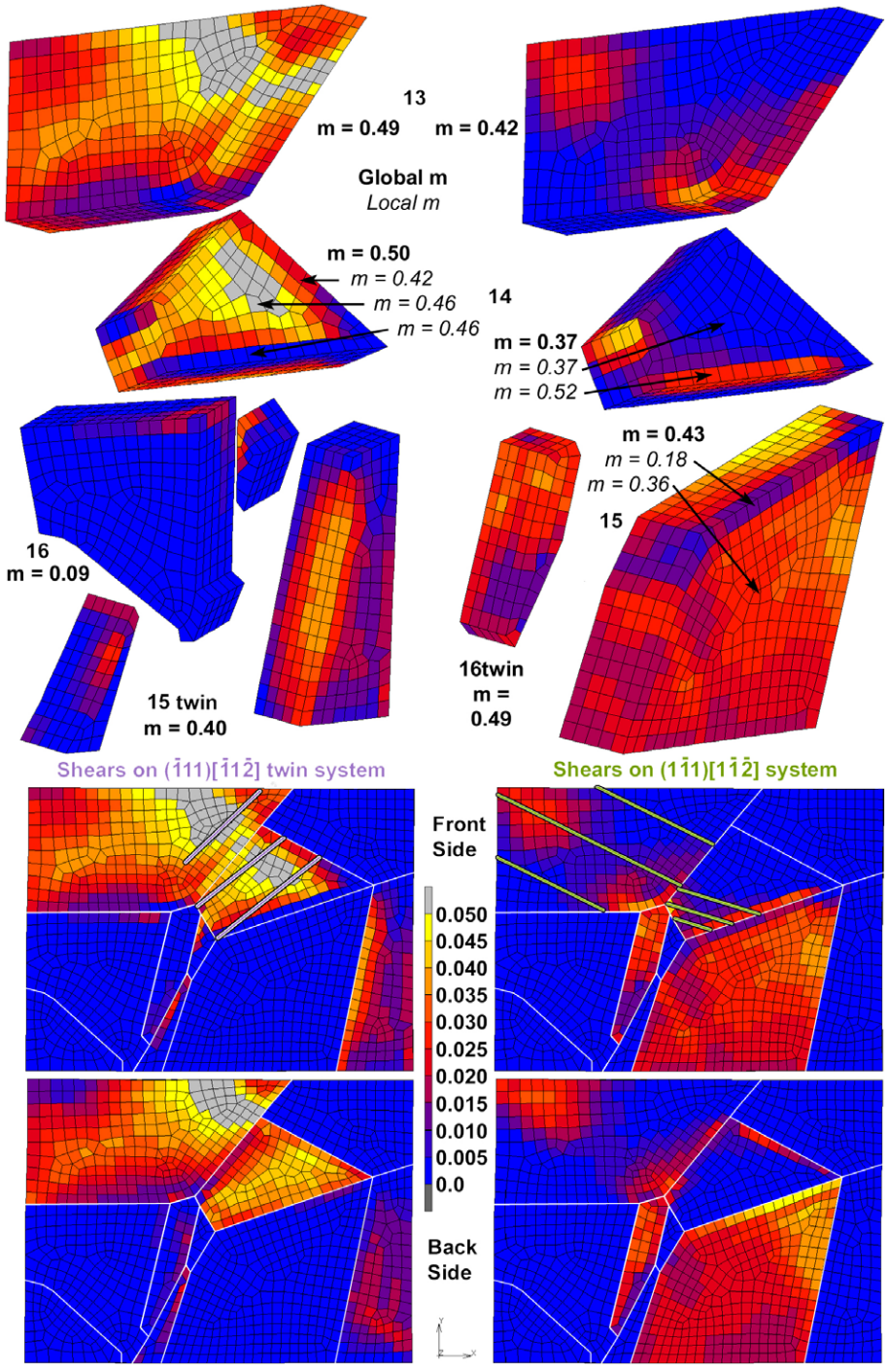

Fig. 14. Shear rates on two active twin systems resolved spatially. Global and some local Schmid factors are noted for the twin systems next to the grain labels.

shear in the FEM model by connecting locations of high shear for twinning with the appropriate plane trace.

In this microstructure, twinning enabled a macroshear band that carried shear across the 13–14 boundary via two twin systems (and also into grain 15, as evident in Figs. 11 and 14), along the systems illustrated with nearly parallel twin plane traces in two grains. The planes and directions are fairly well aligned too; for the (−111) (purple) plane, κ and ψ are 16 and 15°, and for the (1–11) (green) plane, they are 20 and 10°, respectively, while the grains are misoriented by 22° about a [3.8, −5.1, 1] axis. This degree of alignment implies that *fip* values for the 13–14 boundary are relatively high, consistent with the alignment of Burgers vectors (*fip* = 1.006, 1.150, and 1.402, for F_1, F_4, and F_7, which are slightly below the mean for cracked boundaries, above the mean for cracked boundaries, and at the mean for intact boundaries, respectively). These *fip* values indicate that the 13–14 boundary was somewhat susceptible to cracking, but the angle between the tensile axis and an estimated boundary normal was significantly larger than the analyzed population, and thus had a lesser degree of Mode I opening force. The shears predicted by the FEM model in grain 13 are qualitatively correct, but not quantitatively, as the SEM ECCI observations show greater activity of the (1–11) (green) twins whose shears cross the boundary, rather than the (−111) (purple) twins that are roughly parallel to it. This enhanced operation of the (1–11) (green) twins had a lower plane normal mismatch (10°) that may have made the 13–14 boundary more transparent for strain transfer, which was not modeled, so this may account for the lack of agreement between the observed twin activation and the model. Thus, local strain history variations in boundary areas have a large influence on the activated slip systems in the grain interior, due to the need for twins to conduct shear in a contiguous manner through the grain interior.

This analysis tentatively suggests that a simple representation of microstructure geometry may be sufficient for semi-quantitative modeling of shears on various slip systems with CP-FEM calculations, which provide information needed to evaluate the *fip* parameters. Consequently, the *fip* parameter may be a robust parameter for a small plastic strain deformation, because the local stress and strain tensors are not dramatically different even in boundary regions from the simple uniaxial deformation assumed in the existing *fip*. Hence, an OIM map, the *fip* and a direction of maximum stress may be sufficient to identify potentially weak boundaries in a real microstructure.

3.4. Application to other materials

To examine the robustness of this approach, the *fip* was evaluated for dislocation creep in a FCC Cobalt based superalloy that shows susceptibility to grain boundary cracking (Boehlert et al., 2008). In these experiments, OIM maps and SEM images were obtained *in-situ* during creep deformation at elevated temperature. Serial sectioning of ruptured specimens showed that cracks were much more developed on the surfaces than in the interiors, implying that the free surface facilitated crack nucleation. The *fip* analysis was effective, particularly when using images where crack *propagation* had not yet occurred, for predicting boundaries that were susceptible to microcracking. Cracked boundaries were predominantly non-Σ boundaries. It is remarkable that the *fip* approach was effective for a completely different alloy system with a different crystal structure and deformation mode.

At present, this approach is also under investigation for commercial purity Ti, and initial experiments also show that the greatest amounts of heterogeneous strain occurs in the few microns adjacent to grain boundaries (Bieler et al., 2008). While is clear that slip transfer depends upon grain boundary geometry details and slip plane orientations, it will be important to further investigate if the slip direction may be the most important parameter for predicting damage *nucleation*.

Finally, the existing *fip* is not based upon the evolution of strain in a neighborhood, which should be an important component of predicting damage nucleation. Thus having confidence in the CP-FEM model's ability to evolve strain with quantitative accuracy is an important prerequisite before an evolutionary damage nucleation parameter could be developed. Prior work has shown that dislocation density based constitutive models (rather than phenomenological CRSS evolution models) can better simulate the heterogeneous strains that develop in ductile metals (Cheong and Busso, 2004, Clayton and McDowell, 2004, Ma et al., 2006a,b). While the (local) model used here may be less credible than a dislocation density based (non-local strain gradient) model, it does show that the crystal plasticity

FEM model returns results that are at least semi-quantitatively consistent with experiments in a material with small plastic strains. This conventional crystal plasticity FEM model of TiAl deformation to 1–2% strain provides a similar level of confidence as dislocation density based models provide for cubic metals with strains larger than 10%. One possible reason for the good and possibly better agreement with experiment in this TiAl microstructure than in the dislocation density based simulations of aluminum bicrystals conducted by Ma et al. (2006a,b), is that the TiAl has a much greater anisotropy than aluminum.

4. Conclusions

Based on this state of knowledge and the above experimental and CP-FEM modeling of TiAl polycrystal microstructures, we can evaluate four of the 19 hypotheses described at the end of section I affirmatively, specifically numbers 2, 3, 4, and 12, which are restated and *justified with results from this analysis in italics*:

2: Large local strains can provide geometric accommodation that can prevent damage nucleation. *Damage nucleation was not observed at locations having the highest local strain (or strain energy) values*.

3: Damage nucleation arises from slip interactions resulting from imperfect slip transfer through a boundary, which leaves residual dislocation content in the boundary plane, and

4: Damage nucleation occurs in particular boundaries where unfavorable slip interactions take place at the boundary to weaken the boundary. *The fracture initiation parameter for the 14–15 grain boundary had a high value, indicating that multiple types of imperfect slip transfer was possible, and damage was caused by a twin system that was especially favored by the local stress/strain state at the boundary, which led to microcrack nucleation*.

12: Slip directions are more influential on damage nucleation than slip planes. *Attempts to incorporate slip planes into fip parameters indicated a much smaller amount of correlation between slip planes and cracked and intact boundary populations than parameters based upon Burgers vector directions*.

Furthermore, this analysis provides evidence that is contrary to hypothesis 1, i.e. damage nucleation was *not* directly correlated to strain energy, for the monotonic deformation conditions investigated here. The strain energy in locations identified by nodes K, F, and G provided more than twice as much strain energy than location C, where cracks nucleated. Regions of high local strain energy did not correspond with large modifications of the global strain tensor, but this may be a symptom of small strain states and significant elastic anisotropy. These data are inconclusive regarding hypothesis 5 (slip interactions at the boundary are more (or less?) important than the magnitude of local strain for predicting damage nucleation), as a local strain maximum occurred in the same grain as the twin system responsible for the microcrack nucleation. Some data were provided that do not support hypothesis 13 (low-Σ boundaries are less likely to accumulate damage than random boundaries), but the observations are insufficient in number to be statistically convincing. Hypotheses 6–11, 14–18 were not, or could not, be evaluated.

Acknowledgements

The experimental part of this research was supported by the Air Force Office of Scientific Research contract number under Grant # F49620-01-1-0116, monitored by Dr. Craig Hartley and by the Michigan State University Composite Materials and Structures Center. T.R.B. acknowledges sabbatical support from the Max-Planck-Institut für Eisenforschung and Michigan State University, and practical help with FEM calculations from Nader Zaafarani, Claudio Zambaldi, and Luc Hantcherli at MPIE. D.E.M. acknowledges sabbatical support from a grant from the Hewlett-Mellon Fund for Faculty Development at Albion College, Albion. MI. Finally, the authors appreciate several insightful comments from reviewers that have enriched this paper.

References

Appel, F., 2005. An electron microscope study of mechanical twinning and fracture in TiAl alloys. Philosophical Magazine 85 (2–3), 205–231.

Arata, J.J.M., Kumar, K.S., Curtin, W.A., Needleman, A., 2002. Crack growth across colony boundaries in binary lamellar TiAl. Materials Science and Engineering A 329, 532–537.
Arsenlis, A., Parks, D.M., Becker, R., Bulatov, V.V., 2004. On the evolution of crystallographic dislocation density in non-homogeneously deforming crystals. Journal of the Mechanics and Physics of Solids 52 (6), 1213–1246.
Ashmawi, W.M., Zikry, M.A., 2003a. Single void morphological and grain-boundary effects on overall failure in FCC polycrystalline systems. Materials Science and Engineering A343, 126.
Ashmawi, W.M., Zikry, M.A., 2003b. Grain boundary effects and void porosity evolution. Mechanics of Materials 35 (3-6), 537.
Balint, D.S., Deshpande, V.S., Needleman, A., Van der Giessen, E., 2005. A discrete dislocation plasticity analysis of grain-size strengthening. Materials Science and Engineering A400, 186–190.
Barabash, R.I., Ice, G.E., Pang, J.W.L., 2005. Gradients of geometrically necessary dislocations from white beam microdiffraction. Materials Science and Engineering A 400, 125–131.
Barlat, F., Brem, J.C., Yoon, J.W., Chung, K., Dick, R.E., Lege, D.J., Pourgoghrat, F., Choi, S.H., Chu, E., 2003. Plane stress yield function for aluminum alloy sheets – Part 1: theory. International Journal of Plasticity 19 (9), 1297–1319.
Bardella, L., 2007. Some remarks on the strain gradient crystal plasticity modelling, with particular reference to the material length scales involved. International Journal of Plasticity 23 (2), 296–322.
Barton, N.R., Dawson, P.R., 2001. On the spatial arrangement of lattice orientations in hot-rolled multiphase titanium. Modelling and Simulation in Materials Science and Engineering 9 (5), 433–463.
Bennett, V.P., McDowell, D.L., 2003. Crack tip displacements of micro structurally small surface cracks in single phase ductile polycrystals. Engineering Fracture Mechanics 70 (2), 185–207.
Bennett, V.P., McDowell, D.L., 2002. Cyclic crystal plasticity analyses of stationary, microstructurally small surface cracks in ductile single phase polycrystals. Fatigue & Fract. Engineering Materials Structure 25 (7), 677–693.
Bhattacharyya, A., El-Danaf, E., Kalidindi, S.R., Doherty, R.D., 2001. Evution of grain-scale microstructure during large strain simple compression of polycrystalline aluminum with quasi-columnar grains: OIM measurements and numerical simulations. International Journal of Plasticity 17 (6), 861–883.
Bieler, T.R., Crimp, M.A., Eisenlohr, P., Yang, Y., Wang L., Ice, G.E., Liu, W., 2008. unpublished research.
Bieler, T.R., Fallahi, A., Ng, B.C., Kumar, D., Crimp, M.A., Simkin, B.A., Zamiri, A., Pourboghrat, F., Mason, D.E., 2005a. Fracture initiation/propagation parameters for duplex TiAl grain boundaries based on twinning, slip, crystal orientation, and boundary misorientation. Intermetallics 13 (9), 979–984.
Bieler, T.R., Goetz, R.L., Semiatin, S.L., 2005b. Anisotropic plasticity and cavity growth during upset forging of Ti–6Al–4V. Materials Science and Engineering A405, 201–213.
Bieler, T.R., Nicolaou, P.D., Semiatin, S.L., 2005c. An experimental and theoretical investigation of the effect of local colony orientations and misorientation on cavitation during hot working of Ti–6Al–4V. Metallurgical and Materials Transactions A 36A (1), 129–140.
Bjerken, C., Melin, S., 2004. A study of the influence of grain boundaries on short crack growth during varying load using a dislocation technique. Engineering Fracture Mechanics 71 (15), 2215–2227.
Boehlert, C.J., Longanbach, S.C., Bieler, T.R., 2008. The effect of thermomechanical processing on the creep behavior of Udimet Alloy 188. Philosophical Magazine A 88 (5), 641–664.
Bollmann, W., 1991. The stress-field of a model triple-line disclamation. Materials Science and Engineering 136, 1–7.
Bollmann, W., 1988. Triple-line disclinations representations, continuity and reactions. Philosophical Magazine A – Physics of Condensed Matter Structure Defects and Mechanical Properties 57 (4), 637–649.
Bollmann, W., 1984. Triple Lines In Polycrystalline Aggregates as Disclinations. Philosophical Magazine A – Physics of Condensed Matter Structure Defects and Mechanical Properties 49 (1), 73–79.
Bollmann, W., 1982. Crystal Lattices, Interfaces, Matrices. Bollmann, Geneva.
Brandon, D.G., 1966. Structure of high-angle grain boundaries. Acta Metallurgica 14, 1479.
Brown, J.A., Mishin, Y., 2007. Dissociation and faceting of asymmetrical tilt grain boundaries Molecular dynamics simulations of copper. Physical Review B 76 (13), Art. No. 134118.
Buchheit, T.E., Wellman, G.W., Battaile, C.C., 2005. Investigating the limits of polycrystal plasticity modeling. International Journal of Plasticity 21 (2), 221–249.
Busso, E.P., Cailletaud, G., 2005. On the selection of active slip systems in crystal plasticity. International Journal of Plasticity 21 (11), 2212–2231.
Cahn, J.W., Mishin, Y., Suzuki, A., 2006. Coupling grain boundary motion to shear deformation. Acta Materialia 54, 4953–4975.
Cao, S.Q., Zhang, J.X., Wu, J.S., Wang, L., Chen, J.G., 2005. Microtexture, grain boundary character distribution and secondary working embrittlement of high strength IF steels. Materials Science and Engineering A392, 203–208.
Chen, S.R., Gray, G.T., 1996. Constitutive behavior of tantalum and tantalum-tungsten alloys. Metallurgical and Materials Transactions A 27 (10), 2994–3006.
Cheong, K.S., Busso, E.P., 2004. Discrete dislocation density modelling of single phase FCC polycrystal aggregates. Acta Materialia 52 (19), 5665–5675.
Cheong, K.S., Busso, E.P., 2006. Effects of lattice misorientations on strain heterogeneities in FCC polycrystals. Journal of Mechanics Physics Solids 54, 671–689.
Cheong, K.S., Smillie, M.J., Knowles, D.M., 2007. Predicting fatigue crack initiation through image-based micromechanical modeling. Acta Materialia 55 (5), 1757–1768.
Clark, W.A.T., Wagoner, R.H., Shen, Z.Y., Lee, T.C., Robertson, I.M., Birnbaum, H.K., 1992. On the criteria for slip transmission across interfaces in polycrystals. Scripta Metallurgica et Materialia 26, 203.
Clayton, J.D., McDowell, D.L., 2003. Finite polycrystalline elastoplasticity and damage: multiscale kinematics. International Journal of Solids Structure 40 (21), 5669–5688.
Clayton, J.D., McDowell, D.L., 2004. Homogenized finite elastoplasticity and damage: theory and computations. Mechanics of Materials 36 (9), 825–847. v. 36(9), 799–824.
Crimp, M.A., Ng, B.C., Simkin, B.A., Bieler, T.R., 2003. Microcrack nucleation and crack propagation in γ tial, defect properties and related phenomena in intermetallic alloys. In: George, E.P., Mills, M.J., Inui, H., Eggeler, G. (Eds.), MRS Proceedings, vol. 753, pp. 143-148.

Davies, P., Randle, V., 2001. Grain boundary engineering and the role of the interfacial plane. Materials Science and Technology 17 (6), 615–626.
Dawson, P.R., Mika, D.P., Barton, N.R., 2002. Finite element modeling of lattice misorientations in aluminum polycrystals. Scripta Materialia 47 (10), 713–717.
de Koning, M., Miller, R., Bulatov, V.V., Abraham, F.F., 2002. Modelling grain-boundary resistance in intergranular dislocation slip transmission. Philosophical Magazine A 82 (13), 2511–2527.
de Koning, M., Kurtz, R.J., Bulatov, V.V., Henager, C.H., Hoagland, R.G., Cai, W., Nomura, M., 2003. Modeling of dislocation-grain boundary interactions in FCC metals. Journal of Nuclear Materials 323 (2–3), 281–289.
Delaire, F., Raphanel, J.L., Rey, C., 2000. Plastic heterogeneities of a copper multicrystal deformed in uniaxial tension: Experimental study and finite element simulations. Acta Materialia 48 (5), 1075–1087.
Diard, O., Leclereq, S., Rousselier, G., Cailletaud, G., 2005. Evaluation of finite element based analysis of 3D multicrystalline aggregates plasticity – application to crystal plasticity model identification and the study of stress and strain fields near grain boundaries. International Journal of Plasticity 21 (4), 691–722.
Dunne, F.P.E., Rugg, D., Walker, A., 2007. Lengthscale-dependent, elastically anisotropic, physically-based hcp crystal plasticity Application to cold-dwell fatigue in Ti alloys. International Journal of Plasticity 23 (6), 1061–1083.
Edwards, D.J., Singh, B.N., Bilde-Sørensen, J.B., 2005. Initiation and propagation of cleared channels in neutron-irradiated pure copper and a precipitation hardened CuCrZr alloy. Journal of Nuclear Materials 352, 154–178.
Espinosa, H.D., Panico, M., Berbenni, S., Schwarz, K.W., 2006. Discrete dislocation dynamics simulations to interpret plasticity size and surface effects in freestanding FCC thin films. International Journal of Plasticity 22 (11), 2091–2117.
Fallahi, A., Kumar, D., Bieler, T.R., Crimp, M.A., Mason, D.E., 2006. The effect of grain boundary normal on predicting microcrack nucleation using fracture initiation parameters in duplex TiAl. Materials Science and Engineering A 432, 281–291.
Farkas, D., 2005. Twinning and recrystallisation as crack tip deformation mechanisms during fracture. Philosophical Magazine 85 (2–3), 387–397.
Fedorov, A.A., Gutkin, M.Y., Ovid'ko, I.A., 2003. Transformations of grain boundary dislocation pile-ups in nano and polycrystalline materials. Acta Materialia 51 (4), 887–898.
Fischer, F.D., Appel, F., Clemens, H., 2003. A thermodynamical model for the nucleation of mechanical twins in TiAl. Acta Materialia 51 (5), 1249–1260.
Floreen, S., Westbrook, H., 1969. Grain boundary segregation and grain size dependence of strength of nickel–sulfur alloys. Acta Metallurgica 17, 1175.
Frary, A., Schuh, C.A., 2003. Combination rule for deviant CSL grain boundaries at triple junctions. Acta Materialia 51 (13), 3731–3743.
Gibson, M.A., Forwood, C.T., 2002. Slip transfer of deformation twins in duplex gamma -based Ti–Al alloys. III. Transfer across general large-angle gamma-gamma grain boundaries. Philosophical Magazine A 82, 1381.
Hao, S., Moran, B., Liu, W.k., Olson, G.B., 2003. A hierarchical multi-physics model for design of high toughness steels. Journal of Computer-Aided Materials Design 10, 99–142.
Hao, S., Liu, W.K., Moran, B., Vernerey, F., Olson, G.B., 2004. Multi-scale constitutive model and computational framework for the design of ultra-high strength, high toughness steels. Computer Methods in Applied Mechanics and Engineering 193, 1865–1908.
Hasnaoui, A, Derlet, PM, Van Swygenhoven, H, 2004. Interaction between dislocations and grain boundaries under an indenter – a molecular dynamics simulation. Acta Materialia 52, 2251–2258.
He, Y., Schwarz, R.B., Darling, T., Hundley, M., Whang, S.H., Wang, Z.M., 1997. Elastic constants and thermal expansion of single crystal gamma-TiAl from 300 to 750 K. Materials Science and Engineering A 240, 157–163.
Heripre, E., Dexet, M., Crepin, J., Gelebart, L., Roos, A., Bornert, M., Caldemaison, D., 2007. Coupling between experimental measurements and polycrystal finite element calculations for micromechanical study of metallic materials. International Journal of Plasticity 23 (9), 1512–1539.
Hirth, J.P., Pond, R.C., Lothe, J., 2006. Disconnections in tilt walls. Acta Materialia 54 (16), 4237–4245.
Horstemeyer, M.F., McDowell, D.L., McGinty, R.D., 1999. Design of experiments for constitutive model selection: application to polycrystal elastoviscoplasticity. Modelling and Simulation in Materials Science and Engineering 7 (2), 253–273.
Hu, D., Huang, A., Jiang, H., Mota-Solis, N., Wu, X.H., 2006. Pre-yielding and pre-yield cracking in TiAl-based alloys. Intermetallics 14 (1), 82–90.
Ice, G.E., Larson, B.C., Tischler, J.Z., Liu, W., Yang, W., 2005. X-ray microbeam measurements of subgrain stress distributions in polycrystalline materials. Materials Science and Engineering A399, 43–48.
Juul-Jensen, D.J., 2005. Local orientation measurements in 3D. Texture and Anisotropy of Polycrystals in Solid State Phenomena 105, 49–54.
Kabir, R., Cornec, A., Brocks, W., 2007. Simulation of quasi-brittle fracture of lamellar gamma TiAl using the cohesive model and a stochastic approach. Computational Materials Science 39 (1), 75–84.
Kalidindi, S.R., Bronkhorst, C.A., Anand, L., 1992. Crystallographic texture evolution in bulk deformation processing of FCC metals. Mechanics and Physics of Solids 40, 537–569.
Kalidindi, S.R., Anand, L., 1993. Large deformation simple compression of a copper single crystal. Metallurgical Transactions A 24, 989–992.
Karaman, I., Sehitoglu, H., Beaudoin, A.J., Chumlyakov, Y.I., Maier, H.J., Tome, C.N., 2000. Modeling the deformation behavior of Hadfield steel single and polycrystals due to twinning and slip. Acta Materialia 48 (9), 2031–2047.
Kawahara, K., Ibaraki, K., Tsurekawa, S., Watanabe, T., 2005. Distribution of plane matching boundaries for different types and sharpness of textures. In: PRICM 5: The Fifth Pacific Rim International Conference On Advanced Materials And Processing, Pts 1-5, Se Materials Science Forum, 475-479, Part 1-5, 3871–3874.
Kim, T., Hong, K.T., Lee, K.S., 2003. The relationship between the fracture toughness and grain boundary character distribution in polycrystalline NiAl. Intermetallics 11 (1), 33–39.
Knaul, D.A., Beuth, J.L., Milke, J.G., 1999. Modeling and measurement of the notched strength of gamma titanium aluminides under monotonic loading. Metallurgical and Materials Transactions A 30 (4), 949–959.

Kobayashi, S., Tsurekawa, S., Watanabe, T., 2005. Grain boundary hardening and triple junction hardening in polycrystalline molybdenum. Acta Materialia 53 (4), 1051–1057.
Kokawa, H., Watanabe, T., Karashima, S., 1981. Sliding behavior and dislocation-structures in aluminum grain-boundaries. Philosophical Magazine A 44, 1239.
Konrad, J., Zaefferer, S., Raabe, D., 2006. Investigation of orientation gradients around a hard Laves particle in a warm-rolled Fe3Al-based alloy using a 3D EBSD-FIB technique. Acta Materialia 54 (5), 1369–1380.
Kumar, D, Bieler TR, Eisenlohr P, Crimp MA, Roters F, Raabe D, 2008, On predicting nucleation of microcracks due to slip-twin interactions at grain boundaries in duplex γ-TiAl. In: Proceedings of Materials Processing Defects 5 held at Cornell July 18–20, 2007, Journal of Engineering Materials and Technology, 130, (2008) 021012.
Lagow, B.W., Robertson, I.M., Jouiad, M., Lassila, D.H., Lee, T.C., Birnbaum, H.K., 2001. Observation of dislocation dynamics in the electron microscope. Materials Science and Engineering A 309, 445–450.
Lebensohn, R.A., Tome, C.N., 1993. A self-consistent anisotropic approach for the simulation of plastic-deformation and texture development of polycrystals – application to zirconium alloys. Acta Metallurgica et Materialia 41 (9), 2611–2624.
Lebensohn, R.A., 2001. N-site modeling of a 3D viscoplastic polycrystal using Fast Fourier Transform. Acta Materialia 49 (14), 2723–2737.
Lehockey, E.M., Palumbo, G., 1997. On the creep behaviour of grain boundary engineered nickel. Materials Science and Engineering A 237, 168–172.
Lejcek, P., Hofmann, S., 2002. Prediction of enthalpy and entropy of grain boundary segregation. Surface and Interface Analysis 33 (3), 203–210.
Lejcek, P., Hofmann, S., Paidar, V., 2003. Solute segregation and classification of [100] tilt grain boundaries in alpha-iron: consequences for grain boundary engineering. Acta Materialia 51 (13), 3951–3963.
Lejcek, P., Paidar, V., 2005. Challenges of interfacial classification for grain boundary engineering. Materials Science and Technology 21 (4), 393–398.
Lim, L.C., Raj, R., 1985. Continuity of slip screw and mixed-crystal dislocations across bicrystals of nickel at 573-K. Acta Metallurgica 33, 1577.
Lin, J., Liu, Y., Dean, T.A., 2005. A review on damage mechanisms, models and calibration methods under various deformation conditions. International Journal of Damage Mechanics 14 (4), 299–319.
Liu, W., Ice, G.E., Larson, B.C., Yang, W., Tischler, J.Z., 2005. Nondestructive three-dimensional characterization of grain boundaries by X-ray crystal microscopy. Ultramicroscopy 103, 199–204.
Liu, W.K., Karpov, E.G., Zhang, S., Park, H.S., 2004. An introduction to computational nanomechanics and materials. Computer Methods in Applied Mechanics and Engineering 193, 1529–1578.
Livingston, J.D., Chalmers, B., 1957. Multiple slip in bicrystal deformation. Acta Metallurgica 5, 322.
Luster, J., Morris, M.A., 1995. Compatibility Of Deformation In Two-Phase Ti-Al Alloys: Dependence On Microstructure And Orientation Relationships. Metallurgical and Materials Transactions A 26, 1745.
Ma, A., Roters, F., 2004. A constitutive model for fcc single crystal based on dislocation densities and its application to uniaxial compression of aluminum single crystals. Acta Materialia 52, 3603–3612.
Ma, A., Roters, F., Raabe, D., 2006a. A dislocation density based constitutive model for crystal plasticity FEM including geometrically necessary dislocations. Acta Materialia 54 (8), 2169–2179.
Ma, A., Roters, F., Raabe, D., 2006b. On the consideration of interactions between dislocations and grain boundaries in crystal plasticity finite element modeling – theory, experiments, and simulations. Acta Materialia 54 (8), 2181–2194.
Mahapatra, R., Girshick, A., Pope, D.P., Vitek, V., 1995. Deformation mechanisms of near-stoichiometric single-phase tial single-crystals – a combined experimental and atomistic modeling study. Scripta Metallurgica et Materialia 33 (12), 1921–1927.
McGarrity, E.S., Duxbury, P.M., Holm, E.A., 2005. Statistical physics of grain-boundary engineering. Physical Review E 71(2), Art. No. 026102 Part 2.
McGinty, R.D., McDowell, D.L., 1999. Multiscale polycrystal plasticity. Journal of Engineering Materials Technology E 121 (2), 203–209.
McMahon, C.J., 2004. Brittle fracture of grain boundaries. Interface Science 12 (2–3), 141–146.
Miller, R.E., Shilkrot, L.E., Curtin, W.A., 2004. A coupled atomistics and discrete dislocation plasticity simulation of nanoindentation into single crystal thin films. Acta Materialia 52 (2), 271–284. 19 v.
Needleman, A., 1987. A continuum model for void nucleation by inclusion debonding. Journal of Applied Mechanics 54, 525–531.
Nemat-Nasser, S., Guo, W.G., 2000. Flow stress of commercially pure niobium over a broad range of temperatures and strain rates. Materials Science and Engineering 284, 202–210.
Nemat-Nasser, S., Ni, L.Q., Okinaka, T., 1998. A constitutive model for fcc crystals with application to polycrystalline OFHC copper. Mechanics of Materials 30 (4), 325–341.
Ng, B.C., Bieler, T.R., Crimp, M.A., Mason, D.E., 2005. Prediction of crack paths based upon detailed microstructure characterization in a near-TiAl Alloy. In: Larsen, J.M., Calcaterra, J.R., Christodoulou, L., Dent, M.L., Hardman, W.J., Jones, J.W., Russ, S.M. (Eds.), Materials Damage Prognosis. TMS, Warrendale, PA, pp. 307–314.
Ng, B.C., Bieler, T.R., Crimp, M.A., 2002. The effect of crystal orientation on crack nucleation and arrest in a near-gamma TiAl alloy. In: Soboyejo, W.O., Lewandowski, J.J., Ritchie, R.O. (Eds.), Mechanisms and Mechanics of Fracture: The John Knott Symposium. TMS, Warrendale, PA, pp. 303–308.
Noronha, S.J., Farkas, D., 2004. Effect of dislocation blocking on fracture behavior of Al and alpha α-Fe: a multiscale study. Materials Science and Engineering A 365, 156–165.
Nye, J.F., 1955a. Physical Properties of Crystals. Clarendon Press, Oxford (p. 145).
Nye, J.F., 1955b. Physical Properties of Crystals. Oxford. Clarendon Press (p. 145).
Orsini, V.C., Zikry, M.A., 2001. Void growth and interaction in crystalline materials. International Journal of Plasticity 17 (10), 1393–1417.
Palumbo, G., King, P.J., Aust, K.T., Erb, U., Litchenberger, P.C., 1991. Grain-boundary design and control for intergranular stress-corrosion resistance. Scripta Metallurgica et Materialia 25, 1775.
Palumbo, G., Lehockey, E.M., Lin, P., 1998. Applications for grain boundary engineered materials. JOM 50 (2), 40–43.

Prasannavenkatesan, R., Li, B.Q., Field, D.P., Weiland, H., 2005. A parallel macro/micro elastoplasticity model for aluminum deformation and comparison with experiments. Metallurgical and Materials Transactions 36A (1), 241–256.
Pyo, S.G., Kim, N.J., 2005. Role of interface boundaries in the deformation behavior of TiAl polysynthetically twinned crystal, in situ transmission electron microscopy deformation study. Journal of Materials Research 20 (7), 1888–1901.
Querin, J.A., Schneider, J.A., Horstemeyer, M.F., 2007. Analysis of micro void formation at grain boundary triple points in monotonically strained AA6022–T43 sheet metal. Materials Science and Engineering A 463 (1–2), 101–106.
Raabe, D., Sachtleber, M., Zhao, Z., Roters, F., Zaefferer, S., 2001. Micromechanical and macromechanical effects in grain scale polycrystal plasticity experimentation and simulation. Acta Metallurgica et Materialia 49, 3433–3441.
Randle, V., 1995. The influence of grain junctions and boundaries on superplastic deformation. Acta Metallurgica et Materialia 43 (5), 1741–1749.
Randle, V., 2004. Twinning-related grain boundary engineering, Acta Materialia 52(14), 4067–4081. Ridley, N., Wang, Z.C., 1997, The effect of microstructure and deformation conditions on cavitation in superplastic materials, Towards Innovation In Superplasticity I, Se Materials Science Forum 233, 63−80.
Randle, V., 2001. The coincidence site lattice and the 'sigma enigma'. Materials Characterization 47, 411–416.
Rezvanian, O., Zikry, M.A., Rajendran, A.M., 2006. Microstructural modeling of grain subdivision and large strain inhomogeneous deformation modes in f.c.c. crystalline materials. Mechanics of Materials 38 (12), 1159–1169.
Rohrer, G.S., Randle, V., Kim, C.-S., Hu, Y., 2006. Changes in the five-parameter grain boundary character distribution in a-brass brought about by iterative thermomechanical processing. Acta Materialia 54, 4489–4502.
Rohrer, G.S., Saylor, D.M., El-Dasher, B.S., Adams, B.L., Rollett, A.D., Wynblatt, P., 2004. The distribution of internal interfaces in polycrystals. Zeitschrift fur Metallkunde 95, 197–214.
Sachtleber, M., Zhao, Z., Raabe, D., 2002. Experimental investigation of plastic grain interaction. Materials Science and Engineering A 336, 81–87.
Saraev, D., Schmauder, S., 2003. Atomic-scale simulations of the interaction between dislocations and tilt grain boundaries in alpha-iron. Physica Status Solidi B – Basic Research 240 (1), 81–90.
Schuh, C.A., Kumar, M., King, W.E., 2003. Analysis of grain boundary networks and their evution during grain boundary engineering. Acta Materialia 51 (3), 687–700.
Sfantos, G.K., Aliabadi, M.H., 2007. Multi-scale boundary element modelling of material degradation and fracture. Computer Methods in Applied Mechanics and Engineering 196 (7), 1310–1329.
Shan, Z.H., Gokhale, A.M., 2004. Digital image analysis and microstructure modeling tools for microstructure sensitive design of materials. International Journal of Plasticity 20 (7), 1347–1370.
Shen, Y., Anderson, P.M., 2006. Transmission of a screw dislocation across a coherent, slipping interface. Acta Materialia 54 (15), 3941–3951.
Simkin, B.A., Ng, B.C., Crimp, M.A., Bieler, T.R., 2007. Crack opening due to deformation twin shear at grain boundaries in near- γ TiAl. Intermetallics 15, 55–60.
Simkin, B.A., Crimp, M.A., Bieler, T.R., 2003a. A factor to predict microcrack nucleation at γ-γ grain boundaries in TiAl. Scripta Materialia 49 (2), 149–154.
Simkin, B.A., Ng, B.C., Bieler, T.R., Crimp, M.A., Mason, D.E., 2003b. Orientation determination and defect analsysis in the near-cubic intermetallic γ-TiAl using SACP, ECCI, and EBSD. Intermetallics 11, 215–223.
Simkin, B.A., Crimp, M.A., 1999. An experimentally convenient configuration for electron channeling contrast imaging. Ultramicroscopy 77 (1–2), 65–75.
Singh, A., King, A.H., 1993. Tables of coincidence orientations for ordered tetragonal L lo alloys for a range of axial ratios. Acta Crystallographica B 49, 266–272.
Solenthaler, C., Bollmann, W., 1986. Between primary and secondary relaxation in a grain-boundary. Materials Science and Engineering A 81, 35–49.
Spearot, D.E., Jacob, K.I., McDowell, D.L., 2004. Non-local separation constitutive laws for interfaces and their relation to nanoscale simulations. Mechanics of Materials 36, 825–847.
Spearot, D.E., Jacob, K.I., McDowell, D.L., 2005. Nucleation of dislocations from [001] bicrystal interfaces in aluminum. Acta Materialia 53 (13), 3579–3589.
Spearot, D.E., Jacob, K.I., McDowell, D.L., 2007. Dislocation nucleation from bicrystal interfaces with dissociated structure. International Journal of Plasticity 23 (1), 143–160.
Spearot, D.E., Capolungo, L., Qu, J., Cherkaoui, M., 2008a. On the elastic tensile deformation of < 100 > bicrystal Interfaces in copper. Computational Materials Science 42 (1), 57–67.
Spearot, D.E., 2008b. Evolution of the E structural unit during uniaxial and constrained tensile deformation. Mechanics Research Communications 35 (1–2), 81–88.
Spowart, J.E., Mullens, H.M., Puchala, B.T., 2003. Collecting and analyzing microstructures in three dimensions: a fully automated approach. JOM 55 (10), 35–37.
Su, J.Q., Demura, M., Hirano, T., 2003. Mechanical behaviour of sigma 3 boundaries in Ni_3Al. Acta Materialia 51 (9), 2505–2515.
Sun, S., Adams, B.L., King, W.E., 2000. Observations of lattice curvature near the interface of a deformed aluminium bicrystal. Philosophical Magazine A 80 (1), 9–25.
Tatschl, A., Kolednik, O., 2003. On the experimental characterization of crystal plasticity in polycrystals. Materials Science and Engineering A 342, 152.
Thorning, C., Somers, M.A.J., Wert, J.A., 2005. Grain interaction effects in polycrystalline Cu. Materials Science and Engineering A 397, 215–228.
Tschopp, M.A., McDowell, D.L., 2007. Asymmetric tilt grain boundary structure and energy in copper and aluminium. Philosophical Magazine 87 (25), 3871–3892.
Tschopp, M.A., Spearot, D.E., McDowell, D.L., 2008. Dislocation nucleation in Sigma 3 asymmetric tilt grain boundaries. International Journal of Plasticity 24 (2), 191–217.
Tschopp, M.A., Spearot, D.E., McDowell, D.L., 2007. Atomistic simulations of homogeneous dislocation nucleation in single crystal copper. Modelling and Simulation in Materials Science and Engineering 15 (7), 693–709.

Tsurekawa, S., Kokubun, S., Watanabe, T., 1999. Effect of grain boundary microstructures of brittle fracture in polycrystalline molybdenum, towards innovation in superplasticity II-3. Se Materials Science Forum 304, 687–692.
Voyiadjis, G.Z., Abu Al-Rub, R.K., Palazotto, A.N., 2004. Thermodynamic framework for coupling of non-local viscoplasticity and non-local anisotropic viscodamage for dynamic localization problems using gradient theory. International Journal of Plasticity 20 (6), 981–1038.
Wang, M.G., Ngan, A.H.W., 2004. Indentation strain burst phenomenon induced by grain boundaries in niobium. Journal of Materials Research 19 (8), 2478–2486.
Watanabe, T., 1984. An approach to grain-boundary design for strong and ductile polycrystals. Res Mechanica 11 (1), 47–84.
Watanabe, T., Tsurekawa, S., 1999. The control of brittleness and development of desirable mechanical properties in polycrystalline systems by grain boundary engineering. Acta Materialia 47 (15–16), 4171–4185.
Watanabe, T., 2000. Grain boundary engineering for high performance structural and functional materials. Journal De Physique IV 10 (P6), 41–46.
Watanabe, T., Tsurekawa, S., 2004. Toughening of brittle materials by grain boundary engineering. Materials Science and Engineering A 387–89, 447–455.
Watanabe, T., Tsurekawa, S., 2005. Prediction and control of grain boundary fracture in brittle materials on the basis of the strongest-link theory, materials structure & micromechanics of fracture iv. Materials Science Forum 482, 55–62.
Wolf, D., 1990. Correlation between structure, energy, and ideal cleavage fracture for symmetrical grain-boundaries in fcc metals. Journal of Materials Research 5 (8), 1708–1730.
Wu, X., Jiang, H., Huang, A., Hu, D., Mota-Solis, N., Loretto, M.H., 2006. Microstructural study of pre-yielding and pre-yield cracking in TiAl-based alloys. Intermetallics 14, 91–101.
Wu, M.S., 1997. Crack nucleation due to dislocation pile-ups at I-, U- and amorphized triple lines. Mechanics of Materials 25, 215–234.
Wu, M.S., He, M.D., 1999. Prediction of crack statistics in a random polycrystal damaged by the pile-ups of extrinsic grain-boundary dislocations. Philosophical Magazine 79 (2), 271–292.
Wu, M.S., Nazarov, A.A., Zhou, K., 2004. Misorientation dependence of the energy of [1–100] symmetrical tilt boundaries in hcp metals: prediction by the disclination-structural unit model. Philosophical Magazine 84 (8), 785–806.
Xu, X.-P., Needleman, A., 1994. Numerical simulations of fast crack growth in brittle solids. Journal of the Mechanics and Physics of Solids 42, 1397–1434.
Yao, Z., Wagoner, R.H., 1993. Active slip in aluminum multicrystals. Acta Metallurgica et Materialia 41 (2), 451–468.
Yoo, M.H., Zou, J., Fu, C.L., 1995. Mechanistic modeling of deformation and fracture-behavior in TiAl and Ti_3Al. Materials Science and Engineering A193, 14–23.
Zaefferer, S., Kuo, J.C., Zhao, Z., Winning, M., Raabe, D., 2003. On the influence of the grain boundary misorientation on the plastic deformation of aluminum bicrystals. Acta Materialia 51 (16), 4719–4735.
Zaafarani, N., Raabe, D., Singh, R.N., Roters, F., Zaefferer, S., 2006. Three-dimensional investigation of the texture and microstructure below a nanoindent in a Cu single crystal using 3D EBSD and crystal plasticity finite element simulations. Acta Materialia 54 (7), 1863–1876.
Zeghad, A., N'Guyen, F., Forest, S., Gourgues, A.F., Bouaziz, O., 2007. Ensemble averaging stress–strain fields in polycrystalline aggregates with a constrained surface microstructure – Part 1 anisotropic elastic behaviour. Philosophical Magazine 87 (8–9), 1401–1424.
Zhang, Z.F., Wang, Z.G., 2003. Dependence of intergranular fatigue cracking on the interactions of persistent slip bands with grain boundaries. Acta Materialia 51 (2), 347–364.